Facies (2024) 70:3
https://doi.org/10.1007/s10347-023-00678-3

ORIGINAL ARTICLE

Molecular fossils in reefal carbonates and sponges of the deep fore reef of Mayotte and Mohéli, Comoro Islands, western Indian Ocean

Joely Marie Maak[1,2] · Daniel Birgel[1] · Joachim Reitner[3] · Eberhard Gischler[4] · Wolf-Christian Dullo[5] · William J. Foster[1] · Jörn Peckmann[1]

Received: 22 January 2023 / Accepted: 17 November 2023 / Published online: 19 December 2023

Abstract

Microbial carbonates are common components of Quaternary tropical coral reefs. Previous studies revealed that sulfate-reducing bacteria trigger microbial carbonate precipitation in supposedly cryptic reef environments. Here, using petrography, lipid biomarker analysis, and stable isotope data, we aim to understand the formation mechanism of microbial carbonate enclosed in deep fore reef limestones from Mayotte and Mohéli, Comoro Islands, which differ from other reefal microbial carbonates in that they contain less microbial carbonate and are dominated by numerous sponges. To discern sponge-derived lipids from lipids enclosed in microbial carbonate, lipid biomarker inventories of diverse sponges from the Mayotte and Mohéli reef systems were examined. Abundant peloidal, laminated, and clotted textures point to a microbial origin of the authigenic carbonates, which is supported by ample amounts of mono-*O*-alkyl glycerol monoethers (MAGEs) and terminally branched fatty acids; both groups of compounds are attributed to sulfate-reducing bacteria. Sponges revealed a greater variety of alkyl chains in MAGEs, including new, previously unknown, mid-chain monomethyl- and dimethyl-branched MAGEs, suggesting a diverse community of sulfate reducers different from the sulfate-reducers favoring microbialite formation. Aside from biomarkers specific for sulfate-reducing bacteria, lipids attributed to demosponges (i.e., demospongic acids) are also present in some of the sponges and the reefal carbonates. Fatty acids attributed to demosponges show a higher diversity and a higher proportion in microbial carbonate compared to sponge tissue. Such pattern reflects significant taphonomic bias associated with the preservation of demospongic acids, with preservation apparently favored by carbonate authigenesis.

Keywords Molecular fossils · Microbial carbonate · Sponge taphonomy · Sulfate-reducing bacteria · Demospongic acids

Introduction

The occurrence of microbial carbonates (microbialites) in deep tropical fore-reef slopes has been reported for several decades. First descriptions of microbialites in deep fore reef slopes by Land and Goreau (1970) and Land and Moore (1980) reported smooth to knobby, laminated crusts from small cavities of Discovery Bay, Jamaica (– 100 m to – 300 m water depth). These structures consisted chiefly of pelleted high-Mg calcite and have been referred to as microstromatolites (Land and Goreau 1970; Land and Moore 1980). Similar carbonates were found in deep fore reef environments of the Belize barrier and atoll reefs (up to – 300 m; James and Ginsburg 1979) and the Red Sea (– 120 m to – 215 m; Brachert and Dullo 1991). Since then, microbial facies have been described in many other reefal environments, for example, the fore reef slopes of Hawaii

✉ Jörn Peckmann
joern.peckmann@uni-hamburg.de

1 Institut für Geologie, Centrum für Erdsystemforschung und Nachhaltigkeit, Universität Hamburg, 20146 Hamburg, Germany

2 Now at MARUM-Zentrum für Marine Umweltwissenschaften, Universität Bremen, 28359 Bremen, Germany

3 Geowissenschaftliches Zentrum, Universität Göttingen, 37077 Göttingen, Germany

4 Institut für Geowissenschaften, Goethe Universität, 60438 Frankfurt am Main, Germany

5 GEOMAR, 24148 Kiel, Germany

and the Huon Gulf (Webster et al. 2009) and cavities within Holocene tropical reefs (Seard et al. 2011).

Microbialites form by the activity of benthic microbial communities (e.g., Riding 1991) and are among the first fossil evidence of life on Earth (Grotzinger and Knoll 1999). The microbial origin of the carbonate was commonly purported based on morphological evidence only. However, such evidence was proven problematic since many of the purported microbial structures can also form abiotically (e.g., Bosak et al. 2004; Jaramillo-Vogel et al. 2023). A commonly robust proxy to verify a microbial origin of carbonate are molecular fossils (lipid biomarkers). Numerous studies of the biomarker inventories of post-glacial microbialites found to include abundant compounds attributed to sulfate-reducing bacteria (Heindel et al. 2010, 2012; Braga et al. 2019; Gischler et al. 2020). Similarly, cryptic microbialite formation in large reef cavities or coastal submarine caves might also be triggered by sulfate-reducing bacteria (Reitner 1993; Guido et al. 2013; Gischler et al. 2017a, b). Among the most specific lipid biomarkers for sulfate-reducing bacteria in reefal environments are terminally branched *iso*- and *anteiso*-C_{15} and C_{17} fatty acids, 10-Me-C_{16} fatty acid, and, particularly, mono-*O*-alkyl glycerol monoethers (MAGEs) with similar alkyl chains as found for fatty acids (Heindel et al. 2012). These lipid biomarkers are also known from cultures of sulfate-reducing bacteria (Rütters et al. 2001; Grossi et al. 2015) and other environmental samples (Hinrichs et al. 2000; Krake et al. 2022). Organoclastic sulfate reduction (i.e., sulfate reduction using organic compounds as electron donors) can lead to carbonate precipitation by an increase in carbonate alkalinity (Zhang 2020) or by the degradation of extracellular polymeric substances (EPS), which leads to a strong release of Ca ions (e.g., Dupraz et al. 2009). Aside from EPS degradation, sponge tissue decay by heterotrophic bacteria might be an additional agent triggering carbonate formation in some reefs environments (Reitner 1993; Reitner et al. 1995; Reitner and Schumann-Kindel 1997; Luo and Reitner 2014, 2016; Gischler et al. 2021).

Generally, sponges are commonly associated with microbialites in modern and ancient reef systems (e.g., Reitner 1993; Gischler et al. 2017b, 2021; Heindel et al. 2018; Lee and Riding 2018; Turner 2021). In modern coral reefs, such as the reef systems associated with the Comoros Archipelago, coralline sponges and demosponges predominate (e.g., Reitner 1993; Reitner et al. 1995; Erpenbeck et al. 2017). The deep fore reefs of Mayotte and Mohéli show deposits of the Last Glacial Maximum and the following deglacial (Dullo et al. 1998), including laminated, clotted, and peloidal microfabrics of carbonate, as well as sponge remains. Demosponges are known for producing the so-called "demospongic acids", which have chain lengths of 24–30 carbon atoms and a typical unsaturation at $\Delta^{5,9}$ (Litchfield et al. 1976; Litchfield and Morales 1976; Morales and Litchfield 1976). The unique double bond position of demospongic acids is added by other features, such as mid-chain methyl-branchings, additional unsaturations, and brominations (e.g., Litchfield et al. 1980; Bergquist et al. 1984; Wijekoon et al. 1984; Carballeira et al. 1989; Lam et al. 1989; de Kluijver et al. 2021). Demospongic acids are named as such after their first discovery in demosponges but were also described from marine mollusks, terrestrial plants, and cnidarians (Kornprobst and Barnathan 2010).

Microbialites of deep fore reef sites have only been analyzed for their molecular fossil inventory once (Braga et al. 2019). Other than in former studies on reefal microbialites (e.g., Heindel et al. 2010, 2012; Braga et al. 2019; Gischler et al. 2020), the reefal carbonates of Mayotte and Mohéli cannot be assigned as pure microbial carbonate; they contain only moderate amounts of microbial carbonate but abundant sponges instead. The sponges appear to be associated with microbialite formation. Consequently, the lipid biomarker inventories of the Mayotte and Mohéli limestones with microbial carbonate (in the following referred to as reefal carbonates) are compared to lipid biomarker inventories of diverse sponges extracted from the Mayotte and Mohéli reef carbonates. In addition to the characterization of the lipid biomarker inventory of the various sponges, the taphonomy and selective preservation of sponge-specific lipid biomarkers (i.e., demospongic acids; Germer et al. 2013) were examined.

Geological setting

The Comoros Archipelago is located between northwestern Madagascar and east Africa (northern Mozambique) and consists of four main islands aligned along an NW–SE axis (Grande Comore, Mohéli, Anjouan, and Mayotte; Fig. 1). The origin of the Archipelago is designated as a volcanic chain developed as a zone of right-lateral tear in the lithosphere (Famin et al. 2020). The Comoros Archipelago is interpreted as the northern boundary between the Lwandle microplate and the Somalia plate (Famin et al. 2020). New morpho-bathymetric data from Tzevahirtzian et al. (2021) suggests that Mayotte and Mohéli represent the oldest islands, while Anjouan and Grande Comore are more recent. Absolute age data of the volcanic rocks of Mayotte range from 7.7 ± 1.0 to 1.49 ± 0.04 Ma, while the volcanic rocks of Mohéli range from 5.0 ± 0.4 to 0.48 ± 0.15 Ma (Nougier and Cantagrel 1983).

Fringing reefs surround the volcanic islands of the Comoros Archipelago to varying extents. A well-developed barrier reef system (up to 2 km wide) additionally encloses Mayotte, including sand aprons. The Mayotte barrier reef represents the only isolated or Darwinian barrier reef system in the Indian Ocean (Guilcher

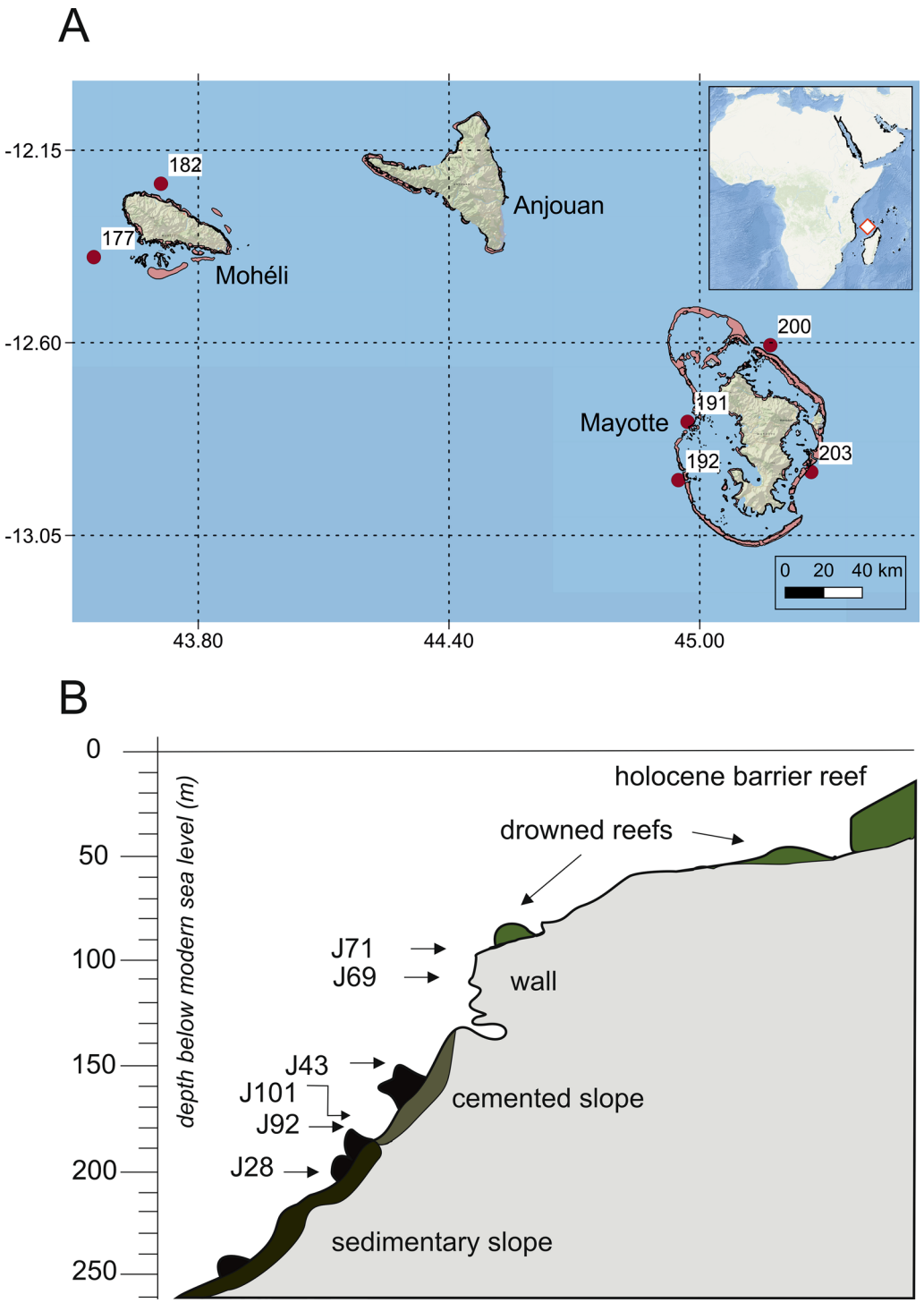

Fig. 1 Map of the Comoros Archipelago (Mohéli, Anjouan, and Mayotte; Grande Comore not shown) in the eastern Indian Ocean (**A**). Sketch showing the general morphology of the Mayotte and Mohéli foreslopes with depth positions of the samples taken (**B**). Sample J28 was collected during dive 177, J43 during dive 182, J69 during dive 191, J71 during dive 192, J92 during dive 200, and J101 during dive 203. Reef locations from UNEP-WCMC (2021); sampling data from Colonna (1994), Colonna et al. (1996), Dullo et al. (1996), and Dullo et al. (1998)

1965, 1971). The volcanic island of Mayotte covers an area of 375 km^2, while the lagoon inside the barrier reef covers about 1500 km^2 with a maximum width of 15 km (Guilcher 1971). About 15 channels (− 50 to − 80 m deep)

connect the lagoon with the open ocean (Guilcher 1971). The several km wide Grande Passe de Ouest is the broadest channel, located at the western margin (Masse et al. 1989). The volcanic island of Mohéli covers about 290 km^2. A fringing reef runs along the total coastal area, and reef platforms surround the island. On the southern side of Mohéli, a partial barrier reef has developed.

The overall morphologies of the foreslopes of Mayotte and Mohéli show strong similarities (Dullo et al. 1996, 1998). The shallow fore reef down to − 20 m water depth is characterized by spurs and grooves that merge into a cliff, a steep detrital talus, and a pre-reef platform at around − 50 m depth (Camoin et al. 1997). Drowned reef terraces occur from − 50 to − 100 m water depth (Dullo et al. 1996, 1998). The drowned reefs form small mounds (up to 3 m) covered predominantly by the coral *Leptoseris* and the green alga *Halimeda* (Dullo et al. 1998). Three central morphological and sedimentary units can be differentiated: an almost vertical wall from − 100 to − 150 m water depth, followed by a cemented slope and a sediment slope below − 150 m depth (Dullo et al. 1996, 1998). This general morphology in the Mayotte and Mohéli foreslopes is similar to other deep fore reefs of barrier and atoll reef systems (e.g., Belize: James and Ginsburg 1979; the Great Barrier Reef: Harris and Davies 1989; or the Maldives: Fürstenau et al. 2010). The almost vertical wall (75°–90°) sharply decreases in inclination between − 160 and − 190 m water depth and forms a cemented slope (Dullo et al. 1998). Both, the cemented slope and wall, consist primarily of well-cemented *Halimeda*-rich and coral-bearing grainstone and packstone (Dullo et al. 1998; Camoin et al. 2004). Foraminifera and coralline algae occur in water depths of − 90 to − 120 m (Camoin et al. 2004). Typical ledge rock is present on the upper slope and the wall, covered by unlithified sediment and living benthic organisms, especially sponges (Dullo et al. 1998). The following sediment slope is characterized by grain sizes from silt (upslope) to sand and gravel (at about − 250 m water depth), while skeletal grains are primarily *Halimeda* plates, which are derived from living crops on top of the terraces (Dullo et al. 1998). On top of the sediment slope, especially along the eastern and southwestern margins, huge blocks of several cubic meters in size occur (Dullo et al. 1998).

The hydrological regime at the Comoros Archipelago is dominated by the southward-flowing Mozambique Current and South Equatorial Current, with a well-established major swell flowing southeastward (Donguy and Piton 1991). Tides are semi-diurnal, and tidal ranges exceed 4 m during spring tides (Masse et al. 1989). The climate of Mayotte and Mohéli is tropical warm and the sea-surface temperatures are bimodal and vary from 25 to 29 °C (Ateweberhan and McClanahan 2010). The lagoonal waters of Mayotte can reach temperatures up to 35 °C. Precipitation is controlled by the monsoon and peaks from November to April (Guilcher 1965).

Materials and methods

The samples analyzed here were collected during several dives in the western Indian Ocean with the research submersible JAGO operated from the surface vessel DEEP SALVAGE I in 1991 (Colonna 1994; Colonna et al. 1996; Dullo et al. 1998; Camoin et al. 2004; Fig. 1A). Samples weighing up to 5 kg were broken off with a large chisel and retrieved from the deep fore reef in water depths ranging from − 60 to − 345 m (Dullo et al. 1998). The examined samples are from individual locations around Mayotte and Mohéli from water depths of − 95 to − 200 m (Fig. 1B). The reefal limestones J69 (− 110 m) and J71 (− 95 m) stem from the western coast of Mayotte, and were sampled approximately 30 km apart from each other. Reefal carbonate samples J69 (87 g) and J71 (69 g) were chosen for biomarker analysis, because they contained microbial carbonate. Dating of the samples was done on collected in situ corals using U/Th-alpha counting and thermo-ionization mass spectrometry (Colonna 1994; Dullo et al. 1998), which resulted in ages of 17.0 ± 1.0 ka (J71) and 33.6 ± 1.0 ka (J69). The carbonate rocks, from which encrusting sponges were sampled, resulted in ages of approximately 12.4 ± 0.5 to 19.0 ± 0.5 ka (Colonna 1994). However, the provided ages could deviate from the real ages due to the incorporation of cement or other artifacts during dating of the corals (Colonna 1994). Therefore, the ages must be taken cautiously and represent only a rough estimate for a timeframe of the MIS3 to deglacial times. The sponges encrusting the carbonate hand samples, mostly still alive at the time of sampling, likely only developed during a much later period. All carbonates and sponges were air-dried immediately after sampling and were stored at room temperature at the University of Göttingen until further analyses. Two thin sections (10 × 15 cm) were prepared from reefal carbonate samples J69 and J71a (Fig. 2) and were analyzed with a ZEISS Axio Scope A1 petrographic microscope. Photomicrographs were taken with a CANON DS126621 digital camera. Scans of the thin sections were made with the CanoScan 9000F Mark II. Subsamples for X-ray diffractometry were taken with a hollow drill from the initial hand samples (J71 and J28; samples were named: J71aM1, J71aM2, J28aM1, and J28aM2). The reefal carbonate samples for lipid biomarker analysis (J69 and J71a) represent subsamples taken with a hollow drill of the larger rock samples; encrusting sponges were avoided during sampling. Sponges analyzed for comparison were removed from the rock samples using appropriate metal instruments that were cleaned with organic solvent beforehand (sponge samples: J28AS1b, J43S1b, J43S2b, J71AS1b,

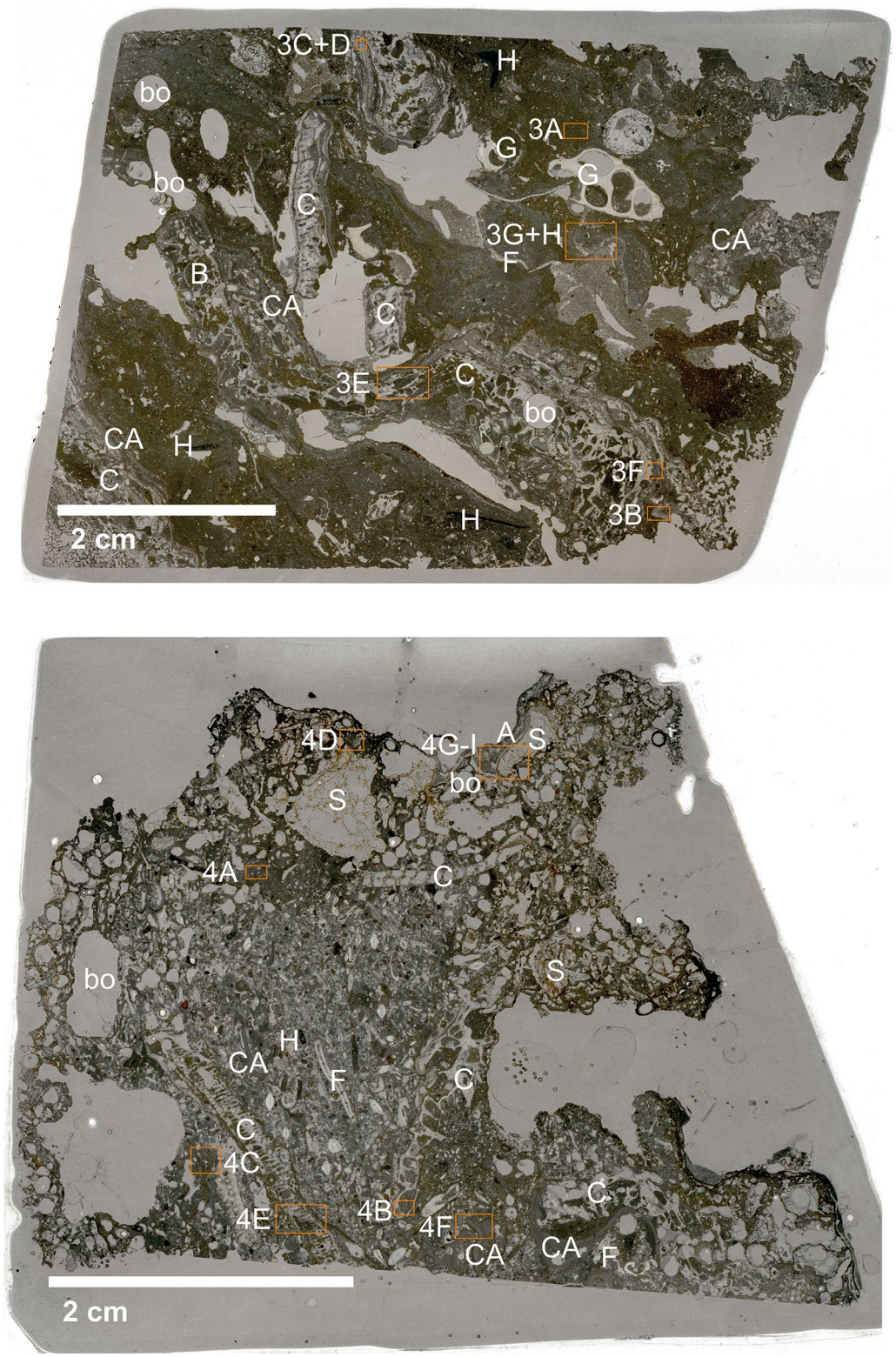

Fig. 2 Thin section scans (top: sample J69; bottom: sample J71a). A: Ascidiacea, bo: boring, B: bivalve, C: coral, CA: coralline algae, F: foraminifera, G: gastropod, H: *Halimeda*, S: sponge. Positions of photomicrographs of Figs. 3 and 4 are indicated

J71AS2b, J71AS3b, J92S1b, J101S1b). All sponges belong to the Subphylum Cellularia, Class Demospongiae (Table 1).

Carbon and oxygen stable isotopic compositions of the reefal carbonates were analyzed in the Isotope Geology Department at the Geoscience Center of the Georg-August-Universität Göttingen (Germany). Forty samples were taken from slabs of the initial hand samples using a hand-held microdrill. Individual microbial carbonate subsamples and inclusions (e.g., *Halimeda* platelets, corals) were collected from samples J27, J28a, J43, J69, J71a, J71b, and J92. Isotope measurements were performed at 70 °C using a Thermo Scientific Kiel IV carbonate device coupled to a Finnigan DeltaPlus gas isotope mass spectrometer. Isotope values are reported as delta values relative to Vienna Pee Dee Belemnite (VPDB) reference standard. X-ray diffractometry measurements were performed using a StoeStadiMP powder X-ray diffractometer with Bragg Bretano geometry and Cu-Kα_1 radiation at the Universität Hamburg (Germany, Institute for Mineralogy). The scan range was 15 to 60 2theta, step size 0.01° 2theta with a scan speed of 0.75° min^{-1}. The magnesium content of calcite was calculated following Goldsmith et al. (1955).

Lipid biomarker analysis of reefal limestones with microbial carbonate and air-dried sponges was conducted at the Institute for Geology at the Universität Hamburg (Germany). Preparation and extraction followed previously published methods (e.g., Birgel et al. 2006; Birgel and Peckmann 2008). All fractions were measured using coupled gas chromatography–mass spectrometry (Thermo Scientific Trace GC Ultra coupled to a Thermo Scientific DSQ II mass spectrometer). The carrier gas was helium with a flow rate of 2.0 ml min^{-1}. The GC–MS was equipped with a 30 m long Agilent HP – 5MS UI or with a Thermo Fisher TG – 5MS-fused silica column (for both columns: inner diameter 0.25 mm, 0.25 µm film thickness). The GC temperature program used for the sponge samples was as follows: injection at 50 °C, 3 min isothermal; from 50 °C to 325 °C at a ramp of 6 °C min^{-1}; 25 min isothermal. For reefal carbonates, the following temperature program was used: injection at 50 °C, 3 min isothermal; from 50 °C to 230 °C at a ramp of 25 °C min^{-1}; from 230 to 325 °C at a ramp of 6 °C min^{-1}; 25 min isothermal. Prior to measurement on the GC–MS, all samples were first measured using a GC-FID (Trace 1310 by Thermo Scientific; H_2 as carrier gas; all other parameters are identical to the measurement with the GC–MS) for quantification. The contents of the biomarkers are given in µg/g (µg/g = µg lipids per g rock or dried sponge). For better comparability of the different samples, wt.% of specified biomarkers as rel.% for alcohols and fatty acids (excluding the contents of the internal standards added) was calculated using the equation from Heindel et al. (2012). To study the structure of branched MAGEs and their compound-specific carbon isotopic compositions, ether cleavage of the monoethers was performed (cf. Hoefs et al. 1997) of an aliquot of the nonderivatized alcohol fraction of samples J71AS1b, J71AS2b, J71AS3b, and J92S1b.

Compound-specific carbon stable isotopes were measured of the ether-cleaved alcohol fractions (J71AS1b, J71AS3b, J92S1b), alcohols (J71a, J69), and fatty acids (J71AS1b, J71AS3b, J92S1b, J71a, J69). Alcohols and fatty acids from the reefal carbonate samples (J69, J71a) were measured at the Universität Hamburg using a gas chromatograph (Agilent 6890) coupled with a Thermo Finnigan Combustion III interface to a Finnigan Delta Plus XL isotope ratio mass

Table 1 Taxonomy of sponge samples used for lipid biomarker analysis

Sample	Order	Family	Genus	Species
J28AS1b	Poecilosclerida?			
	Lithistida	Desmanthidae	*Desmanthus*	*Desmanthus incrustans?*
J43S1b	?			
J43S2b	Poecilosclerida	Microcionina	*Cyamon*	
J71AS1b	Haplosclerida	Chalinidae	*Haliclona?*	
J71AS2b	Poecilosclerida	Microcionina	*Rhabderemiidae?*	
	Clionaida	Spirastrellidae	*Spirastrella*	
	Clionaida	Clionaidae	*Cliona*	
J71AS3b	Tetractinellida	Thoosidae	*Thoosa (Clionidae)*	
	Haplosclerida	Chalinidae	*Haliclona?*	
	Agelasida	Agelasidae	*Agelas*	*Agelas* sp.
J92Slb	Halichondrida?			
	Haplosclerida	Phloeodictyidae	*Aka*	*Aka* sp.
	Poecilosclerida	Myxillidae?		
J101S1b	Hadromerida	Tethyidae	*Tethya*	*Tethya* sp.

spectrometer (GC-IRMS). GC conditions were identical to the conditions using the GC–MS. Compound-specific isotopes of the ether-cleaved alcohols and the remaining fatty acid fractions (J71AS1b, J71AS3b, J92S1b) were measured at MARUM (Universität Bremen) using an Agilent 6890 GC coupled via a Thermo Finnigan Combustion III to a Thermo Finnigan MAT 253 isotope mass spectrometer (GC-IRMS). The following temperature program was used: injection at 50 °C, 2 min isothermal; from 50 to 320 °C at a ramp of 12 °C min^{-1}; 35 min isothermal. Compound-specific carbon isotope values are reported as delta values relative to Vienna Pee Dee Belemnite (VPDB) reference standard. All $\delta^{13}C$ values of fatty acids and alcohols were corrected for the addition of carbon during derivatization.

A cluster analysis using the Bray–Curtis similarity matrix was applied to identify differences between the biomarker inventories of the sponges and the reefal carbonates. Prior to statistical analysis, a percent transformation and a log transformation were performed to standardize the data and reduce the influence of the most abundant biomarkers. The similarity profile test (SIMPROF) was applied to identify significant differences between the clusters (Clarke et al. 2008). For the SIMPROF test, 999 permutations were applied and the chosen significance level was 0.05. The two different sample types were then analyzed through a similarity percentages routine (SIMPER). The sample types and not the identified clusters were used to better discern the characteristic biomarkers of sponges and reefal carbonates. The analyses were performed in PRIMER version 7 (PRIMER-e, 2017) and the results of the SIMPER test were plotted using OriginPro 2019b (OriginLab Corporation, Northampton, MA, USA).

Results

Microfacies

Sample J69 (Figs. 2, 3) is chiefly composed of corals, which were commonly penetrated by boring sponges or bivalves. Among the corals, *Porites* and cf. *Leptoseris* are most abundant. Coralline algae, *Peyssonnelia* sp., and acervulinid foraminifera encrust the coral fragments and accumulations of detritus (Fig. 3E). Other skeletal components are subordinate and contain foraminiferal tests, gastropod and bivalve shell fragments, bryozoan fragments, echinoderm fragments, sponge spicules, and *Halimeda* platelets. Foraminifera genera include *Nummulites* and *Cycloclypeus*, as well as the order Miliolida, which only occur in low quantity. Generally, the matrix is composed of detrital micrite and peloidal micrite with well-defined peloids (Fig. 3A, B). The zones of peloidal micrite are irregular and unevenly laminated (Fig. 2). Occasionally, aragonite cement was found as fans of fibrous crystals and individual acicular, needle-like crystals (Fig. 3C, D). Due to coralline algal layers and peyssonneliacean algae layers showing continuous growth into the other facies (Fig. 3F, G), sample J69 has a bindstone texture.

Sample J71a (Figs. 2, 4) contains various body fossils. Among the highly diverse taxa preserved, foraminifera are most abundant and include in increasing abundance planktonic foraminifera, miliolids, and nummulitids. Corals (*Leptoseris fragilis*; Dullo et al. 1998) and coralline algae account for the highest quantity of skeletal carbonate (Fig. 4E, F). Cavities filled with sponge spicules are abundant (Fig. 4G, H). Laminae of ascidian spicules are present on top of the cavities filled with sponge spicules (Fig. 4I). Since no structure of the ascidian spicules is evident, they cannot be assigned to specific taxa. This is likely due to the dissolution and recrystallization of the originally aragonitic spicules (cf. Matthews 1966). Generally, sample J71a is grain-supported with a micritic matrix. The matrix is either detrital or peloidal and occasionally clotted (Fig. 4A–D). Some parts of the matrix show peloids in a detrital matrix (Fig. 4B). The high percentage of large-sized components (corals with lengths of up to 1.9 cm; coralline algae with lengths of up to 0.9 cm) allows the classification of sample J71a as rudstone.

Isotope patterns and mineralogy of reefal carbonates

Carbon and oxygen stable isotopes of reefal carbonates show a relatively large spread (Fig. 5). Reefal carbonate $\delta^{18}O$ values range from −2 to +1‰ (average -0.3 ± 0.8‰), and $\delta^{13}C$ values range from 0.2 to 4.5‰ (average $+2.6 \pm 0.7$‰) and fall in the field of marine carbonates (cf. Andres et al. 2006). A change in $\delta^{13}C$ and $\delta^{18}O$ values of the microbialites with increasing water depth is apparent. The samples taken at −95 and −110 m below water level (J69 and J71) show a mean $\delta^{13}C$ value of $+2.4 \pm 0.7$‰ and a mean $\delta^{18}O$ value of -0.7 ± 0.4‰ ($n = 26$). Other samples taken at greater depths (−150 to −200 m water depth) yielded higher $\delta^{13}C$ values of $+3.2 \pm 0.4$‰ and higher $\delta^{18}O$ values of $+0.7 \pm 0.2$‰ ($n = 12$). The slight increase is probably a result of rising water temperatures from the deeper to the shallower sites.

Powder X-ray diffractometry of the reefal carbonates revealed $MgCO_3$ mol% contents ranging from 3.6 to 19 (average 15 ± 6.5 $MgCO_3$ mol%; Table 2). Compared to other reefal microbialites, the $MgCO_3$ content of high-Mg calcite of the Mayotte and Mohéli reefal carbonates is similar or slightly lower (Reitner 1993; Gischler et al. 2017b, 2020).

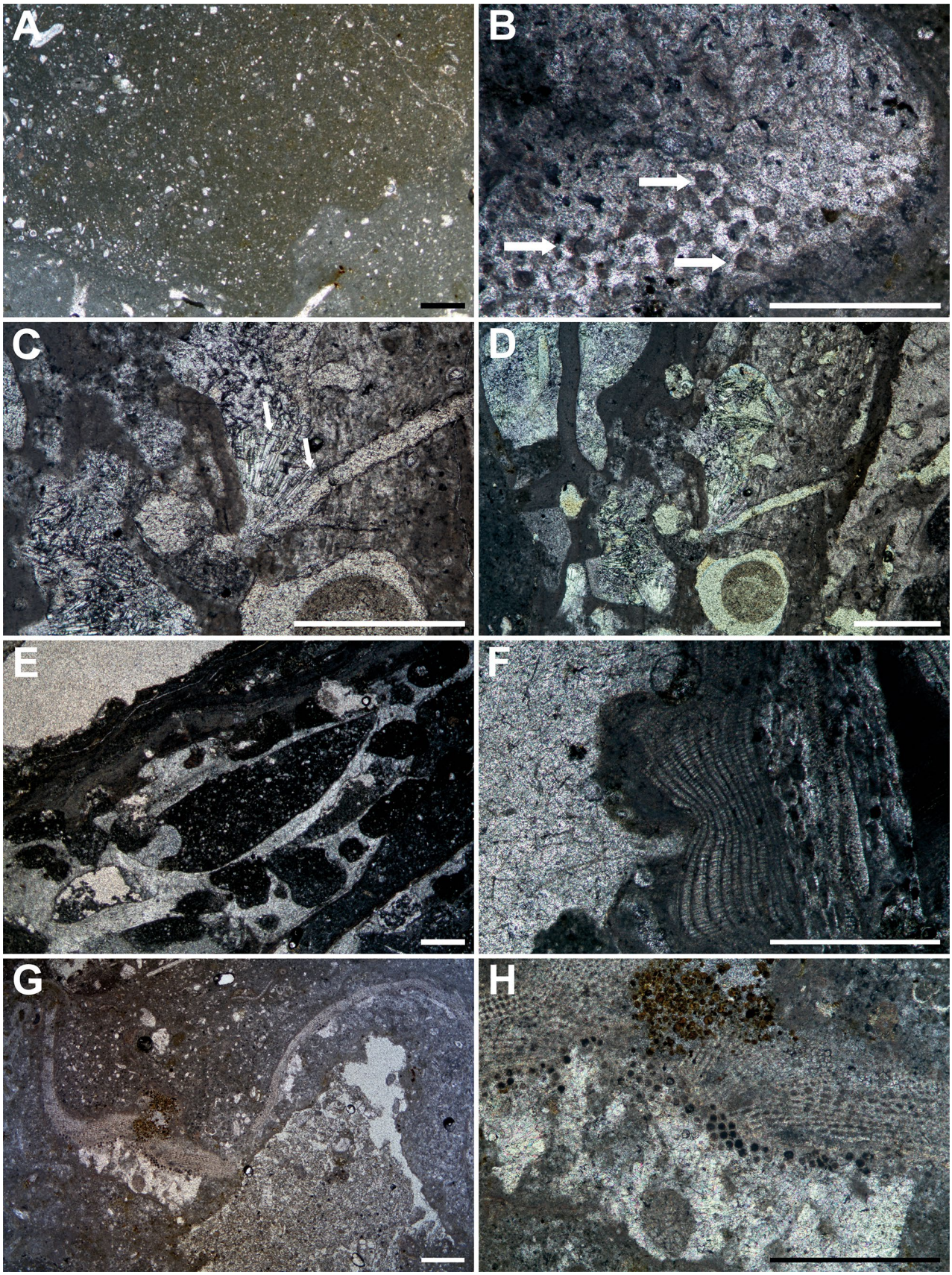
A
B
C
D
E
F
G
H

◂**Fig. 3** Photomicrographs of microfabrics (**A**–**D**) and components (**E**–**H**) in sample J69; all plane-polarized light except (**D**). **A** Matrix of detrital micrite. **B** Peloids (arrows) in ubiquitous microsparitic matrix. **C** Acicular cement. Arrows highlight flat crystal terminations, which indicate aragonite mineralogy. **D** Cement under cross-polarized light. **E** Bored coral. **F** Coralline algal encrustation on coral. **G** Overview of peyssonneliacean algae layers overlaying detrital matrix. **H** Detail of (**G**). Scale bars: 500 µm

Lipid biomarker inventory and compound-specific carbon stable isotopes of reefal carbonates and sponges

The biomarker inventory is composed of various fatty acids, sterols, and non-isoprenoidal *sn* − 1-mono-*O*-alkyl glycerol monoethers (MAGEs). Due to the absence of source-diagnostic biomarkers and generally low contents of biomarkers in the hydrocarbon and ketone fractions, these fractions are not further discussed. The most abundant compounds in sponges are fatty acids (72–737 µg/g dry weight), followed by sterols (2.8–116 µg/g dry weight), and MAGEs (0.52–106 µg/g dry weight). Fatty acids predominate in the extracts of the reefal carbonates (2.5–10 µg/g rock), while alcohols only show minor contents (0.30 and 2.3 µg/g rock) with sterols being the major compound in the alcohol fractions (0.17 and 1.7 µg/g rock). MAGEs only contribute to a minor portion of the alcohols in the reefal carbonate samples (0.03 and 0.23 µg/g rock).

Fatty acids comprise chain lengths from C_{12} to C_{30}. In all samples, $C_{16:0}$ and $C_{18:0}$ show the highest abundance. Short-chain *n*-fatty acids comprise 22–210 µg/g dry weight in the sponge samples and 0.85–2.4 µg/g rock in the reefal carbonate samples (14–50 wt.% and 19–30 wt.%, respectively), while long-chain *n*-fatty acids comprise 4.3–125 µg/g dry weight in the sponge samples and 0.65–1.1 µg/g rock in the reefal carbonate samples (2–24 wt.% and 9–23 wt.%, respectively).

Terminally branched and mid-chain branched fatty acids are abundant in all samples and comprise 25 to 425 µg/g dry weight in the sponge samples and up to 4.4 µg/g rock in the reefal carbonate samples (up to 54 wt.% and up to 36 wt.%, respectively). Mono- and di-unsaturations are common in most of the samples, with the di-unsaturations at the $\Delta^{5,9}$ position of the long-chain fatty acids. Total contents of di-unsaturated long-chain fatty acids range from 0 to 4.4 µg/g dry weight (0 to 1.9 wt.%, respectively) in the sponge samples and up to 1.2 µg/g rock (9.5 wt.%, respectively) in the reefal carbonate samples.

Whereas short-chain *n*-fatty acids ($< C_{20}$) in the reefal carbonates yielded uniform $\delta^{13}C$ values of -23 ± 0.9‰ (J71a) and -24 ± 1.0‰ (J69), long-chain *n*-fatty acids ($\geq C_{24}$) vary between -23 ± 1.9‰ (J71a) and -25 ± 1.2‰ (J69). Generally, the terminally branched fatty acids have slightly higher $\delta^{13}C$ values than short-chain *n*-fatty acids. In detail, *iso*-fatty acids have average values of − 22‰, while *anteiso*-fatty acids are slightly heavier (− 20‰). In the sponge samples, short-chain *n*-fatty acids yielded $\delta^{13}C$ values of -21 ± 1.1‰ (J71AS1b), -22 ± 0.9‰ (J71AS3b), and -22 ± 1.5‰ (J92S1b). Long-chain *n*-fatty acids show similar $\delta^{13}C$ values as short-chain fatty acids (-21 ± 0.2‰ in sample J71AS3b; -18 ± 1.3‰ in sample J92S1b). In contrast to the reefal carbonates, terminally branched *iso*- and *anteiso*-fatty acids in sponge samples show almost no $\delta^{13}C$ offset (av. values: -22 ± 1.6‰). $\delta^{13}C$ values of fatty acids specific for sulfate-reducing bacteria range from − 25 to − 19‰ (average: − 22‰) in sponge samples and from − 22 to − 20‰ (average: − 21‰) in reefal carbonate samples. Other, mid-chain methyl-branched fatty acids range from − 29 to − 16‰ in sponges (average: − 21‰) and from − 23 to − 18‰ in reefal carbonates (average: − 20‰). $\delta^{13}C$ values of demospongic acids vary from − 22 to − 18‰ (average: -20 ± 1.2‰) in reefal carbonate sample J71a. Carbon isotopes of demospongic acids were only measured in one sponge sample (J71AS3b, $C_{25:2\Delta5,9}$-acid), which shows a $\delta^{13}C$ value of − 18‰. Due to contamination, only the biomarkers in the fatty acid fraction from sponge sample J43S1b could be identified.

The majority of MAGEs detected in the sponge and reefal carbonate samples of Mayotte and Mohéli were previously detected in other reefal carbonates (Heindel et al. 2010, 2012; Braga et al. 2019). Among them are terminally branched, short-chain *iso*- and *anteiso*-MAGEs, and 10-Me-C_{16} MAGE. The previously known MAGEs are complemented by novel, not yet described MAGEs in some sponge samples (J28AS1b, J71AS1b, J71AS2b, J71AS3b, and J92S1b). The latter compounds include dimethyl-branched C_{14} and C_{16} MAGEs, as well as monomethyl-branched C_{15}, C_{17}, C_{18}, and C_{22} MAGEs at various positions (see Table 3 for details). Di-*O*-alkyl glycerol diethers (DAGEs), which are commonly found together with MAGEs (e.g., Grossi et al. 2015), are not present in any of the sponge or reefal carbonate samples, which agrees with their scarcity in other reefal carbonates (cf. Heindel et al. 2012).

$\delta^{13}C$ values of MAGEs for reefal carbonate J71a range from − 21 to − 20‰, while $\delta^{13}C$ values of *n*-MAGEs and terminally branched MAGEs in sponge samples range from − 23 to − 21‰ (Table 3). The novel-described MAGEs in the sponge samples show higher variability, ranging from − 25‰ (sample J71AS1b) to − 17‰ (sample J92S1b; see also Table 3 for details). Since the various MAGEs in the sponge samples were co-eluting and their mass spectra equivocal, isotope values were measured for their ether-cleaved alkanes only. The *n*-alkanes yielded after ether cleavage may have been derived from *n*-MAGEs and *n*-alcohols, however, saturated *n*-alcohols and terminally branched alcohols contribute only to a minor part of the biomarker

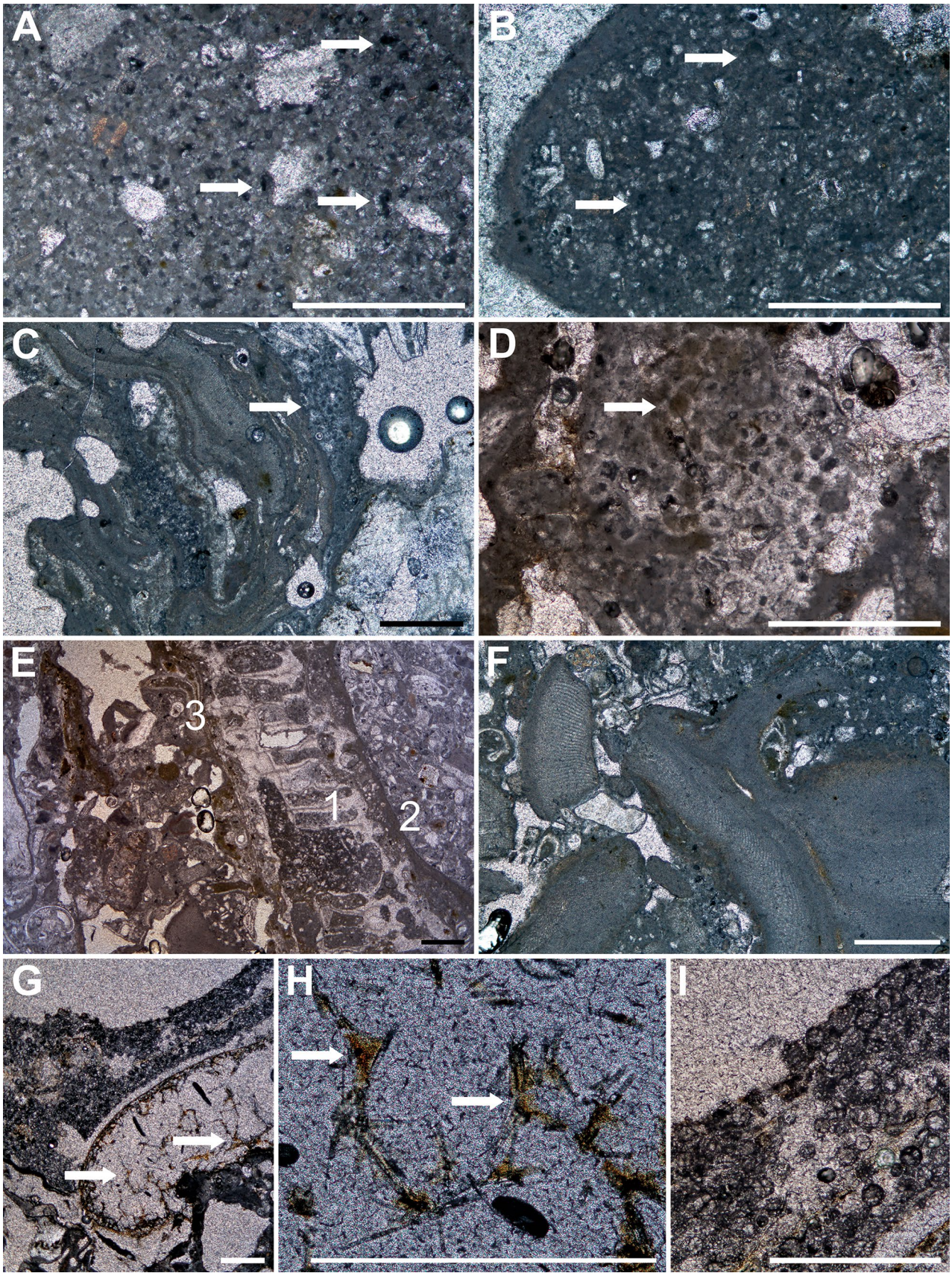
A
B
C
D
E
3
1
2
F
G
H
I

◂**Fig. 4** Photomicrographs of microfabrics (**A**–**D**) and components (**E**–**I**) in sample J71a; all plane-polarized light. **A** Peloidal texture within a matrix of detrital micrite. Arrows point to peloids. **B** Close-up of an internal filling of a boring structure. Arrows indicate peloids. **C** Clotted matrix (arrow) on coralline algae. **D** Peloidal (arrow) texture with foraminifera test (right). **E** Coral fragments (1) encrusted by coralline algae (2) and peyssonneliaceans (3). **F** Coralline algae embedded in fragments of skeletal carbonate and detrital quartz. **G** Cavity filled with sponge spicules (arrows point to spicules). **H** Close-up of sponge spicules (arrows). **I** Crusts of ascidian spicules on top of the cavity. Scale bars: 500 µm

inventory and mid-branched alcohols are not present (except for 10-Me-C_{16}-ol).

Apart from aliphatic compounds, cyclic terpenoids are present in the samples. Sterols were detected in all sponge and reefal carbonate samples and yielded very high contents of 2.9 to 116 µg/g dry weight (3.6 to 33 wt.% of all compounds measured, respectively) in the sponge samples and up to 1.7 µg/g rock (up to 14 wt.%, respectively) in the reefal carbonate samples. Among the sterols, cholestanol and stigmastanol are most abundant in most samples. Compound-specific $\delta^{13}C$ values of sterols vary from − 27 to − 20‰ in the reefal carbonate samples. Hopanols are only minor compounds in sponge samples with up to 9.5 µg/g dry weight (2.3 wt.%, respectively) and are absent in the reefal carbonates.

To discern molecular signatures of the sponge microbiome and the reefal carbonates, cluster analysis is used (Fig. 6). Cluster analysis revealed that the samples can be subdivided into three groups, dominated by specific biomarkers. The highest similarities are between the two reefal carbonate samples J71a and J69, representing the first group. The second group contains sponge samples J71AS1b and J71AS2b, and the third group contains sponge samples J71AS3b, J92S1b, and J28AS1b. The SIMPER test shows that reefal carbonates and sponges are both dominated by *n*-C_{16}-acid and *n*-C_{18}-acid (Fig. 7). The next most abundant biomarkers for reefal carbonates are *iso*- and *anteiso*-C_{15}-acid, while sponges show higher contents of *n*-C_{17}-acid and *iso*-C_{17}-acid (Fig. 7).

Interpretation and discussion

Microbial signatures in reefal limestones and sponges of Mayotte and Mohéli

Aside from the predominating fine-grained matrix and detrital particles, peloidal and more rarely irregularly laminated and/or clotted textures are present in the reefal carbonate. These textures are typically of microbial origin, commonly observed in other reefal microbialites (e.g. Braga et al. 2019) or stromatolites (Folk and Chafetz 2000; Riding and Tomás 2005). Peloidal and clotted textures are obviously no ultimate proof of a microbial origin, but with respect to reefal microbialites such microtextures have commonly been found to co-occur with abundant microbial lipid biomarkers. Some unspecific lipids, which may be produced by phyto- and zooplankton or bacteria, are common in the Mayotte samples (most sterols; Fig. 8; e.g., Volkman 1986, Volkman et al. 1989; average 31 wt.%). However, other biomarkers are of intermediate to high specificity and can be assigned to sulfate-reducing bacteria. These include *iso*- and *anteiso*-C_{15} and C_{17} and 10-Me-C_{16} fatty acids (e.g., Taylor and Parkes 1983; Elvert et al. 2003) and various MAGEs (e.g., Grossi et al. 2015). MAGEs are known to be produced by various thermophilic bacteria, including sulfate-reducing bacteria (Rütters et al. 2001; Grossi et al. 2015; Vinçon-Laugier et al. 2016, 2017). MAGEs are not exclusively produced by sulfate-reducing bacteria, but could also be synthesized by aerobic bacteria (Hernandez-Sanchez et al. 2014). However, the MAGEs found in the reefal carbonates of Mayotte mirror the distribution of MAGEs in previously studied reefal microbialites (cf. Heindel et al. 2010, 2012). The novel MAGEs observed in the Mayotte and Mohéli sponges, however, have not been described from any cultured bacteria to date and could be synthesized by other microorganisms as well. Lipid biomarkers of sulfate-reducing bacteria are accompanied by branched fatty acids at positions Δ^5 and Δ^9, thought to be associated with sponge-specific microorganisms (Thiel et al. 1999), and unsaturated long-chain fatty acids associated with demosponges ("demospongic acids", e.g., Litchfield et al. 1976).

Deep fore reef deposits—metazoan and microbial engineers of complex carbonate lithologies

Complex carbonate lithologies along the deep fore reefs of Mayotte and Mohéli formed at a few tens of meters of water depth during the Last Glacial Maximum and early deglaciation. The carbonate facies of the two studied reefal carbonates agrees with a paleo-water depth of some tens of meters since corals adapted to greater water depths (*Leptoseris*) are abundant (cf. Wells 1954; Schlichter and Fricke 1991; Kahng et al. 2010). The reefal limestones of the Mayotte barrier reef are characterized by a framework of zooxanthellate corals and sponge remains, encrusted by coralline red algae, and overlain by structureless and partially irregular laminated crusts of microbial carbonate. The close association of reefal microbialites and sponge remains in the deep fore reef of Mayotte suggests that bacterial activity associated with sponge tissue decay may have contributed to carbonate precipitation, since degradation of sponges has been shown to favor the precipitation of micrite (Reitner 1993; Reitner et al. 1995; Reitner and Schumann-Kindel 1997; Luo and Reitner 2014, 2016; Gischler et al. 2021).

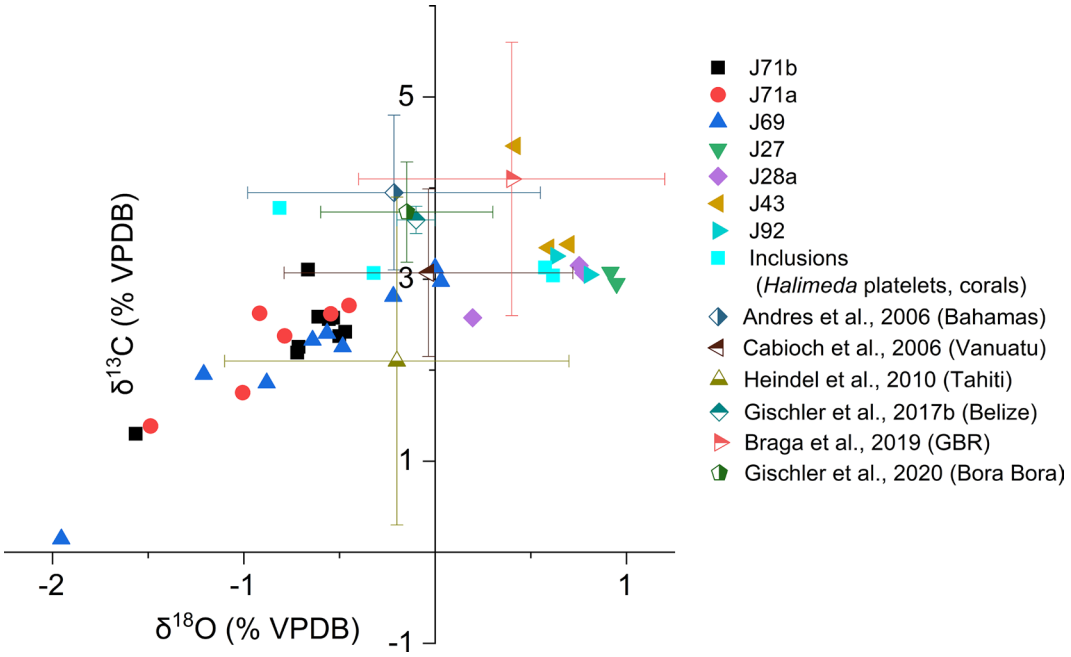

Fig. 5 Cross plot of $\delta^{18}O$ and $\delta^{13}C$ values vs. VPDB of the reefal carbonate, including previously published values by Andres et al. (2006), Cabioch et al. (2006), Heindel et al. (2010), Gischler et al. (2017b), Braga et al. (2019), and Gischler et al. (2020). Published isotope data are indicated by average values and respective variabilities are indicated by bars

Table 2 X-ray diffractometry results

	J71aM1	J71aM2	J28aM1	J28aM2
d [Å] (highest Peak)	2.9820	2.9859	2.9830	3.0275
mol% $MgCO_3$	19	18	19	3.6

Due to their close association with corals and sponges, lipid biomarker analyses of the reefal carbonates are potentially problematic. The complex mixtures of carbonate facies and invertebrate remains could not be separated for analyses, therefore, the biomarker inventories of the reefal limestones

Table 3 Unusual non-isoprenoidal *sn* − 1-mono-*O*-alkyl glycerol monoethers (MAGEs) in samples J71a (reefal carbonate), J71AS1b (sponge), J71AS3b (sponge); contents in µg/g rock or µg/g dw (dry weight); relative percentage referred to the total amount of lipids detected, compound-specific carbon stable isotopes

Compound	J71a		J71AS1b		J71AS3b	
	µg/g rock (wt.%)	$\delta^{13}C$ (‰)	µg/g dw (wt.%)	$\delta^{13}C$ (‰)	µg/g dw (wt.%)	$\delta^{13}C$ (‰)
MAGE (*n*/*iso*/*anteiso*) C_{14} to C_{24}	0.13 (1.1%)	−21 ± 0.2	38 (4.8%)	−22 ± 0.6	10 (2.1%)	−22 ± 0.8
MAGE-7,11-dime-C_{14} and MAGE-6,12-dime-C_{14}			2.3 (0.29%)		0.32 (0.07%)	
MAGE-7-Me-C_{15} or MAGE-9-Me-C_{15} and MAGE-6-Me-C_{15} or MAGE-10-Me-C_{15}			0.46 (0.06%)		0.22 (0.05%)	
MAGE-?-Me-$C_{16:1}$			3.2 (0.40%)		0.30 (0.06%)	
MAGE-10-Me-C_{16}	0.07 (0.60%)	−21	56 (7.0%)	−21	9.1 (1.9%)	−21
MAGE-8,13-dime-C_{16} or MAGE-4,9-dime-C_{16}			1.9 (0.24%)	−22	0.47 (0.10%)	
MAGE-8,14-dime-C_{16} or MAGE-3,9-dime-C_{16}			1.0 (0.13%)	−22	0.14 (0.03%)	
MAGE-8, 7-Me-C_{17} or MAGE-9, 10-Me-C_{17}			0.6 (0.08%)		0.19 (0.04%)	−23
MAGE-9-, 8-, 7-Me-C_{18} or MAGE-10-, 11-, 12-Me-C_{18}			1.5 (0.18%)	−25	0.62 (0.13%)	−22
MAGE-8-, 7-, 6-Me-C_{22} or MAGE-17-, 16-, 15-Me-C_{22}					0.96 (0.20%)	−20

Compound-specific stable isotopes for sponge samples from the ether-cleaved fractions were accounted to *n*- and terminally branched alcohols or MAGEs according to the individual abundance of the biomarkers

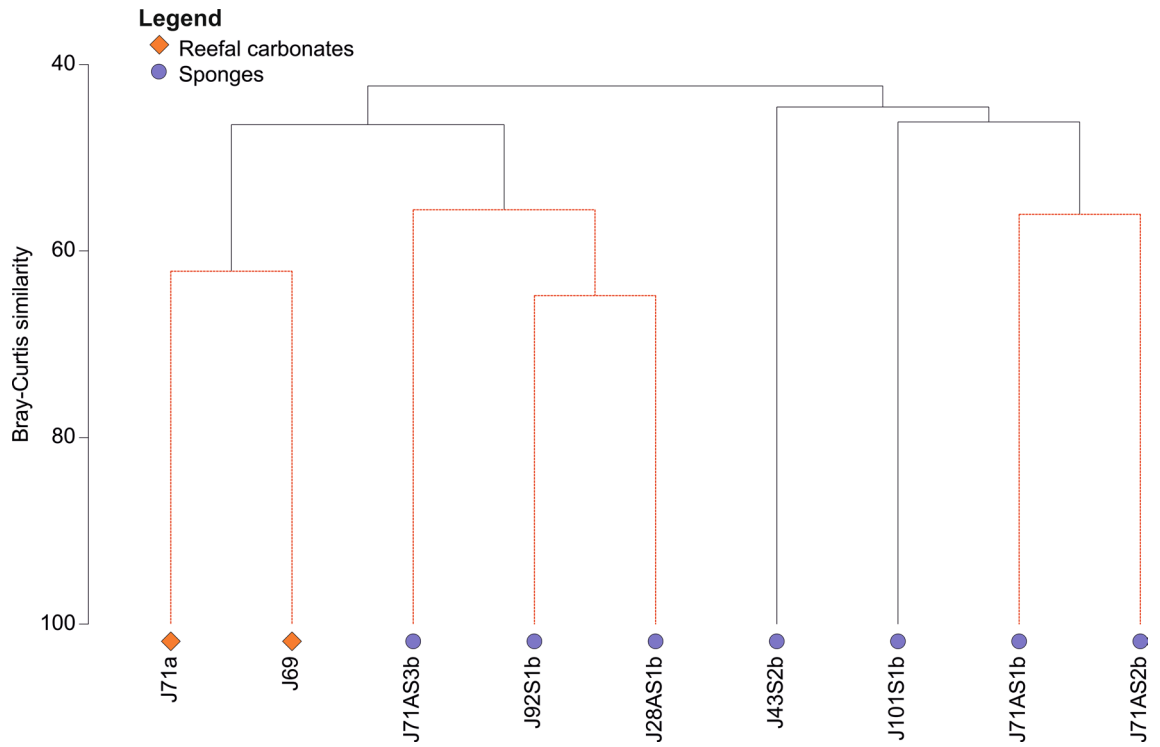

Fig. 6 Result of a cluster analysis of sponge and reefal carbonate samples. The dendrogram together with the SIMPROF test identified three clusters that are statistically different. Prior to cluster analysis, all biomarker data were standardized and log-transformed. The clusters formed identically when removing all biomarkers under 0.2 percent contribution

with microbial carbonate should be interpreted with caution. Particularly, the close association of sponges with reefal carbonates is problematic for biomarker analysis since microorganisms comprise up to 40% of the sponge volume (Taylor et al. 2007). Due to the high abundance and diversity of microbes associated with sponges, the total lipid contents are on average 60 times higher in the sponge samples than in reefal carbonates; such comparison is necessarily problematic since it puts extracts from rocks with extracts of dry biomass into perspective. Overall, to assess the contribution of sponges to the lipid inventory of the Mayotte and Mohéli reefal carbonates, a more elaborated approach became necessary.

How to discern signatures of sponge microbiome and microbial carbonate

Results from the cluster analysis (Fig. 6) indicate that reefal carbonate samples J71a and J69 are similar with regard to their biomarker inventories. In contrast, the similarities between the reefal carbonate sample J71a and their associated sponges from the same hand sample are only minor. Due to their similar biomarker inventories, the reefal carbonate samples seem to have formed under the same conditions, even though both samples were located approximately 30 km apart from each other, stem from different water depths, and have different ages (cf. Colonna 1994; Dullo et al. 1998). The lack of a stronger similarity between the reefal carbonate samples and the sponge samples indicates that any potential bias in the biomarker inventory of the reefal carbonates induced by associated sponges is apparently small despite the high lipid content of the latter.

Like microfacies, the biomarker inventories of the reefal carbonates suggest a strong impact of bacterial activity on carbonate formation. The reefal carbonate samples yielded on average a higher proportion of biomarkers assigned to sulfate-reducing bacteria than sponges (Fig. 8). Still, lipids derived from sulfate-reducing bacteria are present as well in all sponge samples in varying proportions. Therefore, contents of specific fatty acids of sulfate-reducing bacteria (*iso*- and *anteiso*-C_{15} and C_{17} and 10-Me-C_{16} fatty acids) are compared to contents of MAGEs from sulfate-reducing bacteria to further discern lipids of sulfate-reducing bacteria in reefal carbonates from those in sponges. Reefal carbonates show 9- to 13-times higher contents of sulfate-reducing bacteria-derived fatty acids compared to MAGEs. In contrast, fatty acid contents in sponge samples are, with one exception (J101S1b), only up to 5-times higher than MAGEs. Since MAGEs and fatty acids are both rapidly degraded, the offset in the observed biomarker contents in reefal carbonates

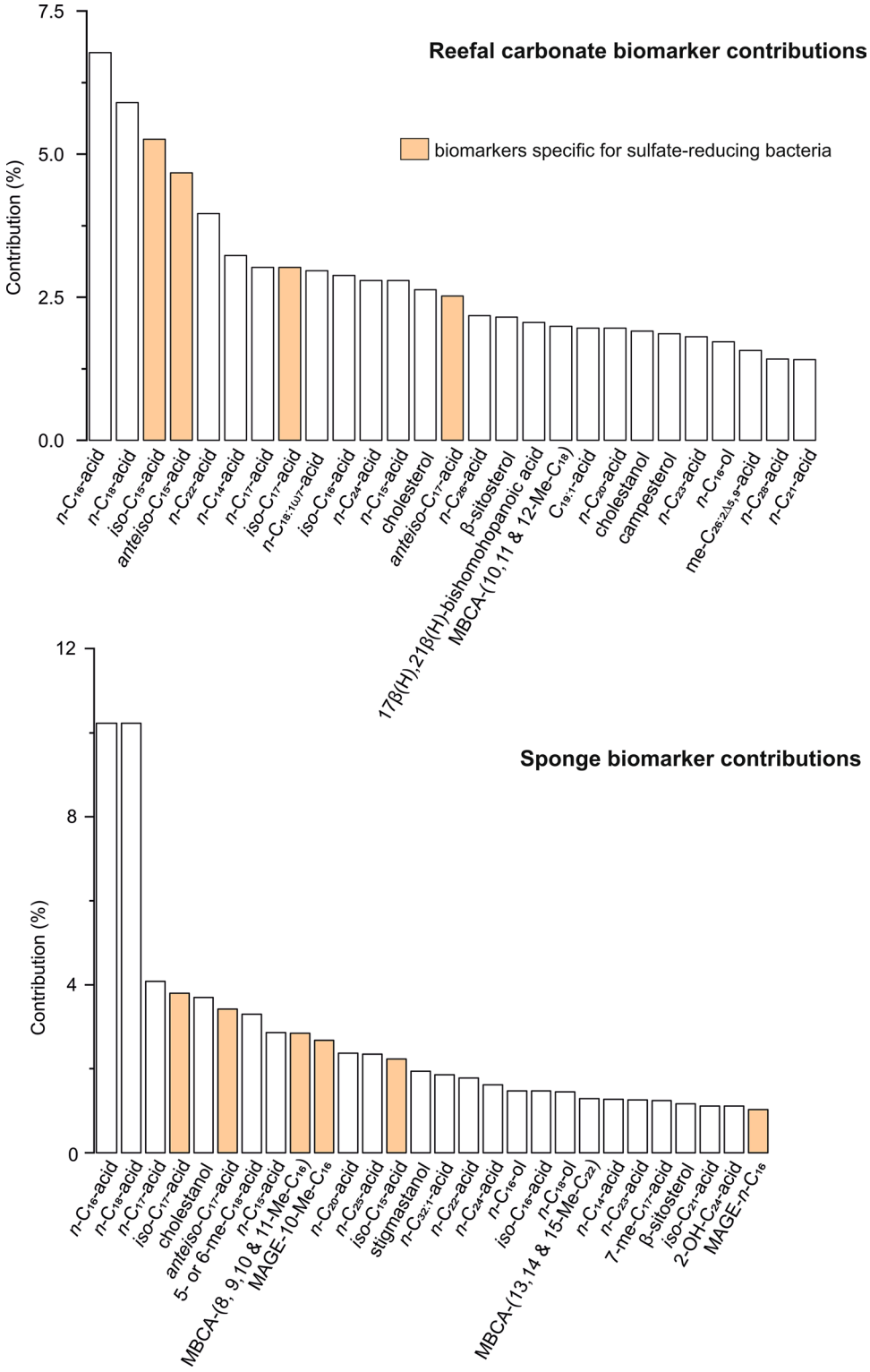

Fig. 7 Average biomarker contributions to the reefal carbonate and sponge samples recognized from the SIMPER analysis. The division in reefal carbonate and sponges is for easier differentiation between the two sample types. Biomarkers attributed to sulfate-reducing bacteria are highlighted in orange. Only the most abundant biomarkers are depicted (75%)

and sponges is unlikely to indicate a preservation bias (cf. Vinçon-Laugier et al. 2018). Taking this into account, the observation of different predominant specific biomarkers in reefal carbonates and sponges, both produced by sulfate-reducing bacteria, reaffirms that most likely different groups of sulfate-reducing bacteria dominate in sponges and the biofilms forming reefal microbialites. Additionally, alkyl chains in MAGEs from sponges are more diverse, including the novel and previously unknown mid-chain monomethyl- and dimethyl-branched MAGEs. The high diversity of alkyl

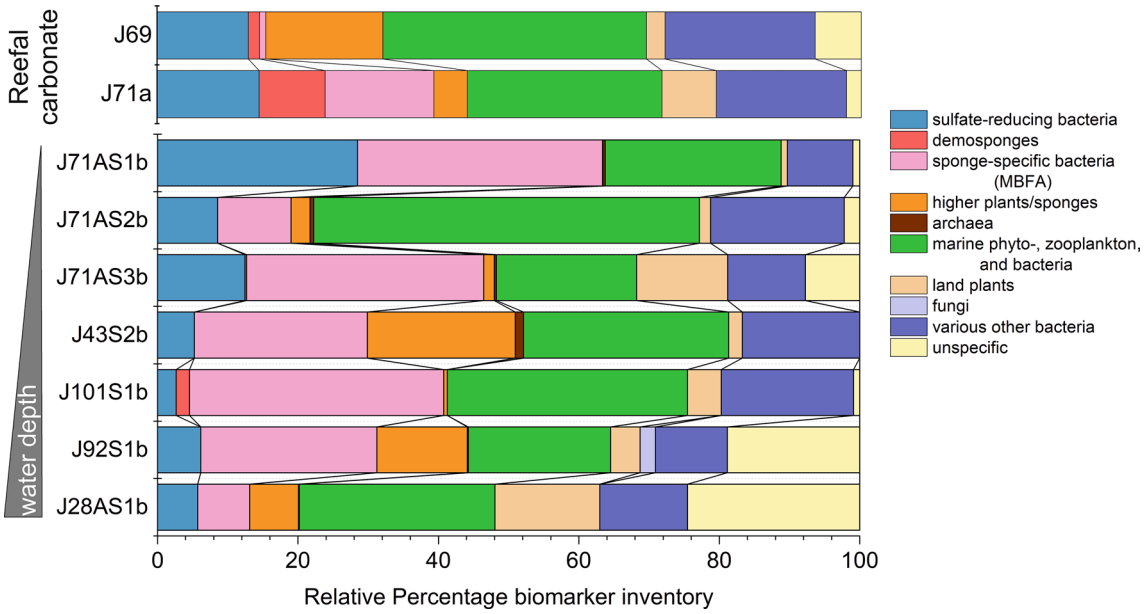

Fig. 8 Biomarker inventory of reefal carbonate samples J69 and J71a and the sponge samples, ordered according to increasing water depth from top to bottom. Demosponges are assigned only by demospongic acids. MBFA: mid-chain branched fatty acid

chains in MAGEs restricted to sponges further suggests a diverse community of sulfate-reducing bacteria in sponges compared to those involved in reefal carbonate formation.

Other potential producers of bacterial lipids in reefal environments are oxygenic phototrophic cyanobacteria. However, cyanobacteria are not known to produce branched fatty acids and MAGEs, and characteristic cyanobacterial biomarkers like heptadecane and heptadecenes (e.g., Wieland et al. 2008) were not detected. Degradation of organic matter in reef cavities by heterotrophic bacteria could have led to the removal of biomarkers of cyanobacteria and could be a reason why such biomarkers are not present in the reefal carbonates (cf. Wieland et al. 2008; Heindel et al. 2010, 2012). It is unlikely that the biomarker inventories of the reefal carbonates reflect the entire benthic microbial communities, but the lack of evidence of the former presence of cyanobacteria in all the biomarker studies conducted to date suggests that cyanobacteria are not abundant in the reef framework where microbialites form (Heindel et al. 2010, 2012; Braga et al. 2019; Gischler et al. 2020). Such lack certainly suggests that cyanobacterial activity has not driven microbialite formation, which would have necessarily resulted in the preservation of the lipids of cyanobacteria.

Additional evidence for sulfate-reducing bacteria as critical agents in microbialite formation comes from the mineralogy of the reefal carbonates. Reefal carbonates of Mayotte and Mohéli are chiefly composed of high-Mg calcite similar to other reefal microbialites. Precipitation of high-Mg calcite is common when high concentrations of dissolved sulfide are present and, as a consequence, a kinetic barrier for the incorporation of magnesium into the calcitic crystal lattice is overcome (e.g., Vasconcelos et al. 1995; Warthmann et al. 2000; Zhang et al. 2012, 2013; Lu et al. 2018). A strongly sulfidic environment can result from a high extent of sulfate reduction in the reef cavities where the carbonates formed. Lower average $MgCO_3$ mol% contents of the reefal carbonates of Mayotte and Mohéli compared to other reefal microbialites probably reflect a greater proportion of detrital material derived from the shallower-water reef system. The $\delta^{13}C$ values observed for the Mayotte and Mohéli reefal carbonates like those of other microbialites are less conclusive though. The average $\delta^{13}C$ value of $2.6 \pm 0.7‰$ and the average $\delta^{18}O$ value of $-0.3 \pm 0.8‰$ of the microbialites phases indicate that carbonate precipitation is not driven by an alkalinity increase caused by the metabolism of sulfate-reducing bacteria (cf. Reitner et al. 2000; Heindel et al. 2010, 2012). Compared to other reefal microbialites, those of Mayotte and Mohéli show slightly lower $\delta^{18}O$ but similar $\delta^{13}C$ values (Andres et al. 2006; Cabioch et al. 2006; Heindel et al. 2010; Gischler et al. 2017b, 2020; Braga et al. 2019; Fig. 5). An explanation for the variations in oxygen and carbon stable isotopes might be the rising water temperatures from the deeper to the shallower sites and incorporation of detritus into the reefal carbonates. Pure microbial carbonate is probably isotopically heavier since the incorporated detrital grains (corals, coralline algae, *Halimeda* platelets, mollusks, bivalves) are more ^{13}C depleted than reefal microbialites (Wefer and Berger 1991; Braga et al. 2019).

Microbialite formation in the fore reef of Mayotte and Mohéli probably took place in small cavities of the reef

system, where marine and terrestrial organic and inorganic detritus accumulated. This caused a locally increased nutrient concentration and developed favorable conditions for sponges. Consequently, both bacterial-derived and sponge-derived lipids in reefal carbonates testify former bacterial activity and the abundance of demosponges. In such cryptic environments, local anoxic conditions in the lower layers of microbial mats or within smaller biofilms developed, favoring conditions for sulfate reduction. Sulfate-reducing bacteria degraded the coral-derived and terrestrial organic matter (including EPS), causing high concentrations of dissolved hydrogen sulfide and Ca ions after EPS decay. Sponge tissue decay might have been an additional agent causing carbonate precipitation. Consequently, microbialites with high-Mg content precipitated. Similar conditions have been put forward to have caused microbialite formation in other reefal environments (cf. Heindel et al. 2010, 2012; Braga et al. 2019; Gischler et al. 2020), however, without the influence of sponges.

Lipids derived from sulfate-reducing bacteria show similar $\delta^{13}C$ values as the biomarkers attributed to demosponges (demospongic acids) and sponge-dwelling bacteria (mid-chain methylated fatty acids; Fig. 9). Such similarity of $\delta^{13}C$ values of lipids of sulfate-reducing bacteria and demosponges was only found for reefal carbonate sample J71a, but not in the sponge samples. Unfortunately, only a single $\delta^{13}C$ value for one demospongic acid could be measured in the sponge samples, which displays a higher $\delta^{13}C$ value compared to lipids derived by sulfate-reducing bacteria (Fig. 9). The MAGEs present in most of the sponge samples are of high diversity, including the previously undescribed MAGEs (Table 3). Typically, a higher diversity of branched MAGEs is synthesized when short-chain fatty acids (octanoate, pyruvate; Vinçon-Laugier et al. 2016) or alkanes ($C_{15:1}$, $C_{16:1}$; Grossi et al. 2015) are consumed, which contradicts the assumption that sulfate-reducing bacteria could have used long-chain substrates like demospongic acids. Considering the results of Grossi et al. (2015) and Vinçon-Laugier et al. (2016), as well as the compound-specific carbon isotopic composition (Fig. 9), sulfate-reducing bacteria probably assimilated organic compounds like short methyl-branched fatty acids. Obviously, other source organisms of the newly described MAGEs than sulfate-reducing bacteria cannot be excluded, since these compounds have not been described in any of the cultured MAGE-producing bacteria (cf. Grossi et al. 2015).

The demospongic acids extracted from the Mayotte and Mohéli fore reef samples show significant taphonomic bias. In the reefal carbonate sample J71a, demospongic acids make up 12 rel.% of all fatty acids, but are absent or sum up to only 0.24 rel.% of all fatty acids in the sponges from the same hand sample (J71AS1b, J71AS2b, J71AS3b; Fig. 10). Generally, out of the eight examined demosponges, only three yielded demospongic acids. In addition to their higher relative abundance, also the variety of demospongic acids is greater in the reefal carbonate sample J71a with nine different demospongic acids present, while sponge sample J71AS3b from the same carbonate rock only yielded one demospongic acid (Fig. 10). Other sponge samples yielded one (J101S1b) or four (J43S1b) demospongic acids. Dating

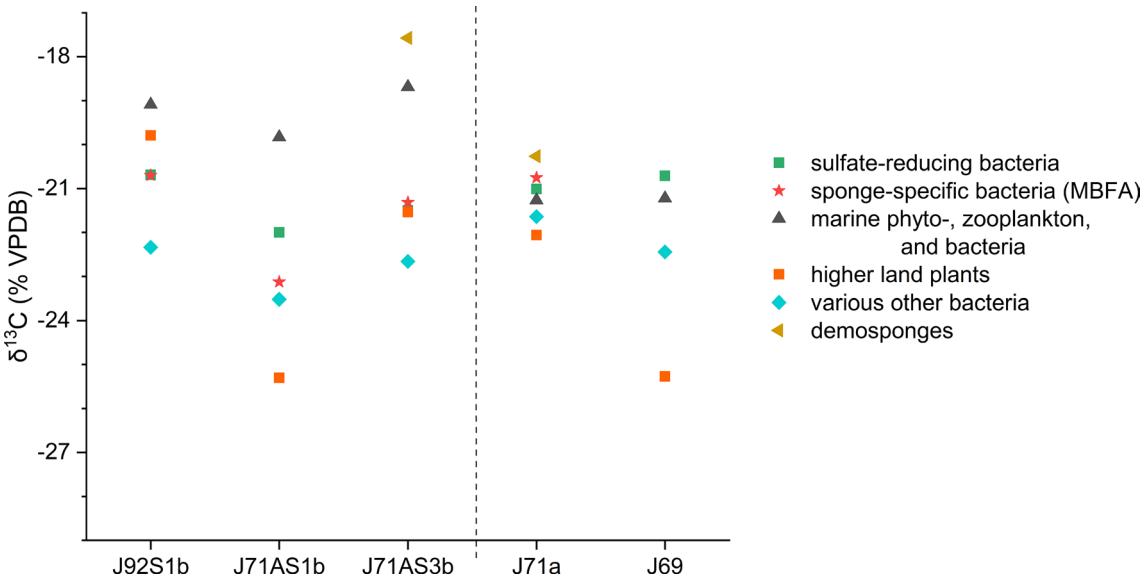

Fig. 9 Compound-specific carbon isotopic compositions of defined groups with their tentative source organisms. All values are depicted without standard deviation. MBFA: methyl-branched fatty acid. Compound-specific stable isotopes for sponge samples from the ether-cleaved fraction were accounted to *n*- and terminally branched alcohols or MAGEs according to the individual abundance of the biomarkers

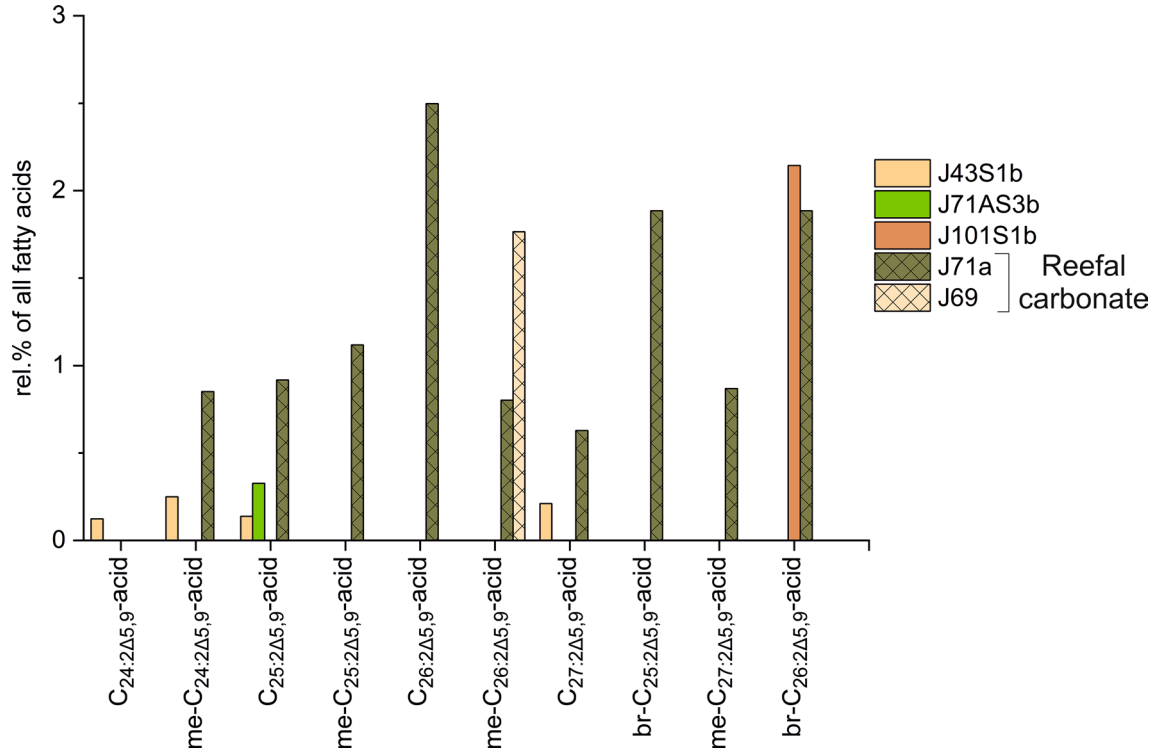

Fig. 10 Contents (rel.% of all fatty acids) of demospongic acids present in sponges (J43S1b, J71AS3b, J101S1b) and reefal carbonates (J71a, J69). Reefal carbonates are displayed with a cross pattern

was carried out on in situ corals; the two sampled reefal carbonates are probably of similar age as the corals, while the encrusting sponges are apparently much younger. The greater variety and abundance of demospongic acids in the reefal carbonate samples suggests better preservation over a longer period of time in the microbial carbonate compared to sponge tissue. Generally, the precipitation of minerals during early diagenesis is expected to promote the preservation of lipids of the microorganisms associated with authigenesis (cf. Peckmann and Thiel 2004). Further, the close association between sponges and carbonates and the higher contents of some of the sponge biomarkers in reefal carbonates indicates a close association of sponges with carbonate precipitation. Similarly, microbialite formation will cause fast incorporation of organic compounds of sponges, impeding their degradation by various heterotrophic bacteria. Our new results confirm that demospongic acids are easily degradable and will vanish in the course of sponge tissue decay within only a few thousand years or less. In reefal carbonates and especially in microbialites, however, demospongic acids can be preserved on geological time scales.

Interestingly, also signatures of endosymbiotic, sponge-dwelling sulfate-reducing bacteria are recorded in the reefal carbonates. The elongation of bacterial fatty acids can be traced in the biomarker inventory of reefal carbonate sample J71a (cf. Rubin-Blum et al. 2019). Isotopic signatures indicate an elongation of *anteiso*-C_{15} fatty acid (− 20‰) over *anteiso*-C_{17} fatty acid (− 20‰), *anteiso*-C_{19} fatty acid (− 19‰), and *anteiso*-C_{21} fatty acid (− 21‰) to me-$C_{24\Delta5,9}$ fatty acid (− 19‰) and me-$C_{25\Delta5,9}$ fatty acid (− 21‰). Such uptake of the *anteiso*-C_{15} and *anteiso*-C_{17}-fatty acids, together with the high amount of biomarkers of sulfate-reducing bacteria in the examined subrecent sponges, indicate that sulfate-reducing bacteria were major symbionts and played a role in sponge nutrition. Sulfate-reducing bacteria as key symbionts in sponges have been described before (e.g., Hoffmann et al. 2005, 2008; Zhang et al. 2015). In contrast, in the Mayotte and Mohéli sponge samples, no incorporation of short-chain fatty acids into the biomass of demosponges was traced. This finding is analog to the stronger degradation processes in sponge tissue deduced from the distribution of demospongic acids, compared to better preservation of lipids in reefal carbonates.

Conclusions

Microbialite formation in the deep fore reef of Mayotte and Mohéli during the MIS3 to deglacial times was favored by sulfate-reducing bacteria. Microbial activity is evidenced by microfabrics but especially by lipid biomarkers and mineralogy. Precipitation of carbonate was probably induced by

the degradation of microbial extracellular polymeric substances and other types of organic matter (sponge tissue, coral mucus), although carbonate species produced from the remineralization of organic matter did not apparently contribute to increased alkalinity. Signatures derived from cyanobacterial activity were not found in the samples analyzed, which is either caused by the absence of cyanobacteria in the depositional environment or the degradation of cyanobacterial biomarkers by heterotrophic bacteria.

The Mayotte and Mohéli reefal carbonates reflect unusual environmental conditions with a high abundance and diversity of sponges associated with the microbial carbonate. Distinguishing between the biomarker inventories of reefal carbonates and sponges is crucial to discern sponge-derived lipids from lipids enclosed in microbial carbonate. Here, statistical analyses and the comparison of biomarker inventories revealed that different groups of sulfate-reducing bacteria were abundant in the sponges and the biofilms or mats forming the microbialites. Demospongic acids show better preservation and higher diversity in reefal carbonates than in sponges. Formation of microbialites apparently resulted in the entombment of lipids and, therefore, favored preservation. However, in degrading sponge tissue and without such entombment, demospongic acids are easily degraded and will vanish from the rock record within a few thousand years. To date, most research on sponge taphonomy has focused on sterols attributed to sponges (cf. Love et al. 2009; Zumberge et al. 2018), whereas only little is known about the taphonomy of demospongic acids. Our study provides first insight into the preservation potential of demospongic acids. Future studies of the taphonomy of demospongic acids, especially in microbialites, will show which variables may affect the preservation potential of these sponge biomarkers.

Acknowledgements We thank Katrin Heindel (Nürnberg) for help with biomarker analyses, Enno Schefuß and Ralph Kreutz (MARUM) for measurements of compound-specific carbon stable isotopes, Carsten Paulmann (Mineralogy, Universität Hamburg) for support during X-ray diffractometry, and Karen Hissmann (GEOMAR) for helping with the exact sampling locations. Insightful comments of two anonymous reviewers helped to improve the manuscript. We acknowledge financial support from the Open Access Publication Fund of Universität Hamburg.

Funding Open Access funding enabled and organized by Projekt DEAL.

Data availability The authors declare that the data supporting the findings of this study are available within the paper.

References

Andres MS, Sumner DY, Reid RP, Swart PK (2006) Isotopic fingerprints of microbial respiration in aragonite from Bahamian stromatolites. Geology 34:973–976. https://doi.org/10.1130/G22859A.1

Ateweberhan M, McClanahan TR (2010) Relationship between historical sea-surface temperature variability and climate change-induced coral mortality in the western Indian Ocean. Mar Pollut Bull 60:964–970. https://doi.org/10.1016/j.marpolbul.2010.03.033

Bergquist PR, Lawson MP, Cambie RC (1984) Fatty-acid composition and the classification of the Porifera. Biochem Syst Ecol 12:375–393. https://doi.org/10.1016/0305-1978(84)90070-X

Birgel D, Peckmann J (2008) Aerobic methanotrophy at ancient marine methane seeps: a synthesis. Org Geochem 39:1659–1667. https://doi.org/10.1016/j.orggeochem.2008.01.023

Birgel D, Thiel V, Hinrichs K-U, Elvert M, Campbell KA, Reitner J, Farmer JD, Peckmann J (2006) Lipid biomarker patterns of methane-seep microbialites from the Mesozoic convergent margin of California. Org Geochem 37:1289–1302. https://doi.org/10.1016/j.orggeochem.2006.02.004

Bosak T, Souza-Egipsy V, Newman DK (2004) A laboratory model of abiotic peloid formation. Geobiology 2:189–198. https://doi.org/10.1111/j.1472-4677.2004.00031.x

Brachert TC, Dullo WC (1991) Laminar micrite crusts and associated foreslope processes, Red-Sea. J Sediment Petrol 61:354–363. https://doi.org/10.1306/D426770D-2B26-11D7-8648000102C1865D

Braga JC, Puga-Bernabéu Á, Heindel K, Patterson MA, Birgel D, Peckmann J, Sánchez-Almazo IM, Webster JM, Yokoyama Y, Riding R (2019) Microbialites in Last Glacial Maximum and deglacial reefs of the Great Barrier Reef (IODP Expedition 325, NE Australia). Palaeogeogr Palaeoclimatol Palaeoecol 514:1–17. https://doi.org/10.1016/j.palaeo.2018.10.007

Cabioch G, Camoin G, Webb GE, Le Cornec F, Molina MG, Pierre C, Joachimski MM (2006) Contribution of microbialites to the development of coral reefs during the last deglacial period: case study from Vanuatu (South-West Pacific). Sediment Geol 185:297–318. https://doi.org/10.1016/j.sedgeo.2005.12.019

Camoin GF, Colonna M, Montaggioni LF, Casanova J, Faure G, Thomassin BA (1997) Holocene sea-level changes and reef development in South-Western Indian Ocean. Coral Reefs 16:247–259. https://doi.org/10.1007/s003380050080

Camoin GF, Montaggioni LF, Braithwaite CJR (2004) Late glacial to post glacial sea levels in the Western Indian Ocean. Mar Geol 206:119–146. https://doi.org/10.1016/j.margeo.2004.02.003

Carballeira NM, Maldonado ME, Rivera E, Porras B (1989) The fatty-acid 4,8,12-trimethyltridecanoic as a common constituent of the phospholipids of the sponge families Spirastrellidae and Clionidae. Biochem Syst Ecol 17:311–314. https://doi.org/10.1016/0305-1978(89)90009-4

Clarke KR, Somerfield PJ, Gorley RN (2008) Testing of null hypotheses in exploratory community analyses: similarity profiles and biota-environment linkage. J Exp Mar Biol Ecol 366:56–69. https://doi.org/10.1016/j.jembe.2008.07.009

Colonna M (1994) Chronologie des variations du niveau marin au cours du dernier cycle climatique (0–140000 ans) dans Ia partie

sud occidentale de l'Ocean Indien. Implications paleoclimatiques et paleoceanographiques. Dissertation, Univ. Provence, Marseille

Colonna M, Casanova J, Dullo WC, Camoin GF (1996) Sea-level changes and $\delta^{18}O$ record for the past 34,000 yr from Mayotte reef, Indian Ocean. Quat Res 46:335–339. https://doi.org/10.1006/qres.1996.0071

de Kluijver A, Nierop KGJ, Morganti TM, Bart MC, Slaby BM, Hanz U, de Goeij JM, Mienis F, Middelburg JJ (2021) Bacterial precursors and unsaturated long-chain fatty acids are biomarkers of North-Atlantic deep-sea demosponges. PLoS ONE 16:e0241095. https://doi.org/10.1371/journal.pone.0241095

Donguy JR, Piton B (1991) The Mozambique channel revisited. Oceanol Acta 14:549–558

Dullo WC, Camoin GF, Blomeier D, Eisenhauer A, Thomassin BA (1996) Sealevel changes and evolution of the foreslopes of the Comoro Islands: Direct observations from submersible. In: Reitner J, Neuweiler F, Gunkel F (eds) Global and regional controls on biogenic sedimentation. I. Reef evolution. Research reports. Göttinger Arbeiten zur Geologie und Paläontologie, Sb 2, Universität Göttingen, Göttingen, pp 19–22. https://oceanrep.geomar.de/id/eprint/291. Assessed 19 Feb 2022

Dullo WC, Camoin GF, Blomeier D, Colonna M, Eisenhauer A, Faure G, Casanova J, Thomassin BA (1998) Morphology and sediments of the fore-slopes of Mayotte, Comoro Islands: direct observations from a submersible. In: Camoin GF, Davies PJ (eds) Reefs and carbonate platforms in the Pacific and Indian oceans. Blackwell Science, Oxford, pp 219–236

Dupraz C, Reid RP, Braissant O, Decho AW, Norman R, Visscher PT (2009) Processes of carbonate precipitation in modern microbial mats. Earth Sci Rev 96:141–162. https://doi.org/10.1016/j.earscirev.2008.10.005

Elvert M, Boetius A, Knittel K, Jørgensen BB (2003) Characterization of specific membrane fatty acids as chemotaxonomic markers for sulfate-reducing bacteria involved in anaerobic oxidation of methane. Geomicrobiol J 20:403–419. https://doi.org/10.1080/01490450303894

Erpenbeck D, Aryasari R, Benning S, Debitus C, Kaltenbacher E, Al-Aidaroos AM, Schupp P, Hall K, Hooper JNA, Voigt O, de Voogd NJ, Wörheide G (2017) Diversity of two widespread Indo-Pacific demosponge species revisited. Mar Biodiv 47:1035–1043. https://doi.org/10.1007/s12526-017-0783-3

Famin V, Michon L, Bourhane A (2020) The Comoros Archipelago: a right-lateral transform boundary between the Somalia and Lwandle plates. Tectonophysics 789:228539. https://doi.org/10.1016/j.tecto.2020.228539

Folk RL, Chafetz HS (2000) Bacterially induced microscale and nanoscale carbonate precipitates. In: Riding RE, Awramik SM (eds) Microbial sediments. Springer Berlin Heidelberg, Berlin, pp 40–49

Fürstenau J, Lindhorst S, Betzler C, Hübscher C (2010) Submerged reef terraces of the Maldives (Indian Ocean). Geo-Mar Lett 30:511–515. https://doi.org/10.1007/s00367-009-0174-2

Germer J, Reitner J, Blumenberg M, Thiel V (2013) Are poriferan biomarkers preserved in the geological record? 9th World Sponge Conference 2013, Fremantle, Western Australia

Gischler E, Birgel D, Brunner B, Eisenhauer A, Meyer G, Buhre S, Peckmann J (2017a) A giant underwater, encrusted stalactite from the Blue Hole, Lighthouse Reef, Belize, revisited: A complex history of biologically induced carbonate accretion under changing meteoric and marine conditions. J Sediment Res 87:1260–1284. https://doi.org/10.2110/jsr.2017.72

Gischler E, Heindel K, Birgel D, Brunner B, Reitner J, Peckmann J (2017b) Cryptic biostalactites in a submerged karst cave of the Belize Barrier Reef revisited: Pendant bioconstructions cemented by microbial micrite. Palaeogeogr Palaeoclimatol Palaeoecol 468:34–51. https://doi.org/10.1016/j.palaeo.2016.11.042

Gischler E, Birgel D, Brunner B, Peckmann J (2020) Microbialite occurrence and patterns in Holocene reefs of Bora Bora, Society Islands. Palaios 35:262–276. https://doi.org/10.2110/palo.2020.026

Gischler E, Fuchs A, Bach W, Reitner J (2021) Massive cryptic microbe-sponge deposits in a Devonian fore-reef slope (Elbingerode Reef Complex, Harz Mts., Germany). PalZ 95:683–707. https://doi.org/10.1007/s12542-021-00581-8

Goldsmith JR, Graf DL, Joensuu OI (1955) The occurrence of magnesian calcites in nature. Geochim Cosmochim Acta 7:212–230. https://doi.org/10.1016/0016-7037(55)90033-8

Grossi V, Mollex D, Vinçon-Laugier A, Hakil F, Pacton M, Cravo-Laureau C (2015) Mono- and dialkyl glycerol ether lipids in anaerobic bacteria: Biosynthetic insights from the mesophilic sulfate reducer *Desulfatibacillum alkenivorans* PF2803T. Appl Environ Microbiol 81:3157–3168. https://doi.org/10.1128/AEM.03794-14

Grotzinger JP, Knoll AH (1999) Stromatolites in Precambrian carbonates: evolutionary mileposts or environmental dipsticks? Annu Rev Earth Planet Sci 27:313–358. https://doi.org/10.1146/annurev.earth.27.1.313

Guido A, Heindel K, Birgel D, Rosso A, Mastandrea A, Sanfilippo R, Russo F, Peckmann J (2013) Pendant bioconstructions cemented by microbial carbonate in submerged marine caves (Holocene, SE Sicily). Palaeogeogr Palaeoclimatol Palaeoecol 388:166–180. https://doi.org/10.1016/j.palaeo.2013.08.007

Guilcher A (1965) Coral reefs and lagoons of Mayotte Island, Comoro Archipelago, Indian Ocean, and of New Caledonia, Pacific Ocean. In*:* Whittard WF, Bradshaw R, (eds) Submarine geology and geophysics: Proceedings of the 17th Symposium of the Coston Research Society, Butterworth, London, pp 21–45

Guilcher A (1971) Mayotte barrier reef and lagoon, Comoro Islands, compared with other barrier reefs, atolls and lagoons in the world. In*:* Stoddart DR, Yonge CM (eds) Regional variation in Indian Ocean coral reefs: Symposium Zoological Society London, London, pp 65–86

Harris PT, Davies PJ (1989) Submerged reefs and terraces on the shelf edge of the Great Barrier Reef, Australia. Coral Reefs 8:87–98. https://doi.org/10.1007/BF00301807

Heindel K, Birgel D, Peckmann J, Kuhnert H, Westphal H (2010) Formation of deglacial microbialites in coral reefs off Tahiti (IODP 310) involving sulfate-reducing bacteria. Palaios 25:618–635. https://doi.org/10.2110/palo.2010.p10-032r

Heindel K, Birgel D, Brunner B, Thiel V, Westphal H, Gischler E, Ziegenbalg S, Cabioch G, Sjövall P, Peckmann J (2012) Post-glacial microbialite formation in coral reefs of the Pacific, Atlantic, and Indian Oceans. Chem Geol 304–305:117–130. https://doi.org/10.1016/j.chemgeo.2012.02.009

Heindel K, Foster WJ, Richoz S, Birgel D, Roden VJ, Baud A, Brandner R, Krystyn L, Mohtat T, Koşun E, Twitchett RJ, Reitner J, Peckmann J (2018) The formation of microbial-metazoan bioherms and biostromes following the latest Permian mass extinction. Gondwana Res 61:187–202. https://doi.org/10.1016/j.gr.2018.05.007

Hernandez-Sanchez MT, Homoky WB, Pancost RD (2014) Occurrence of 1-O-monoalkyl glycerol ether lipids in ocean waters and sediments. Org Geochem 66:1–13. https://doi.org/10.1016/j.orggeochem.2013.10.003

Hinrichs K-U, Summons RE, Orphan V, Sylva SP, Hayes JM (2000) Molecular and isotopic analysis of anaerobic methane-oxidizing communities in marine sediments. Org Geochem 31:1685–1701. https://doi.org/10.1016/S0146-6380(00)00106-6

Hoefs M, Schouten S, De Leeuw JW, King LL, Wakeham SG, Sinninghe Damsté J (1997) Ether lipids of planktonic archaea in the

marine water column. Appl Environ Microbiol 63:3090–3095. https://doi.org/10.1128/aem.63.8.3090-3095.1997
Hoffmann F, Larsen O, Thiel V, Rapp HT, Pape T, Michaelis W, Reitner J (2005) An anaerobic world in sponges. Geomicrobiol J 22:1–10. https://doi.org/10.1080/01490450590922505
Hoffmann F, Røy H, Bayer K, Hentschel U, Pfannkuchen M, Brümmer F, de Beer D (2008) Oxygen dynamics and transport in the Mediterranean sponge *Aplysina aerophoba*. Mar Biol 153:1257–1264. https://doi.org/10.1007/s00227-008-0905-3
James NP, Ginsburg RN (1979) The seaward margin of Belize barrier and atoll reefs. Spec Publ Int Assoc Sedimentol 3:1–191. https://doi.org/10.1002/9781444304510.ch5
Jaramillo-Vogel D, Braga JC, Negga HA, Vennemann T, De Boever E, Schaegis J-C, Rime V, Atnafu B, Kidane T, Foubert A (2023) Pleistocene aragonite crust diagenesis mimics microbialite fabrics (Danakil Depression, Ethiopia). Sediment Geol 446:106341. https://doi.org/10.1016/j.sedgeo.2023.106341
Kahng SE, García-Sais JR, Spalding HL, Brokovich E, Wagner D, Weil E, Hinderstein L, Toonen RJ (2010) Community ecology of mesophotic coral reef ecosystems. Coral Reefs 29:255–275. https://doi.org/10.1007/s00338-010-0593-6
Kornprobst J-M, Barnathan G (2010) Demospongic acids revisited. Mar Drugs 8:2569–2577. https://doi.org/10.3390/md8102569
Krake N, Birgel D, Smrzka D, Zwicker J, Huang H, Feng D, Bohrmann G, Peckmann J (2022) Molecular and isotopic signatures of oil-driven bacterial sulfate reduction at seeps in the southern Gulf of Mexico. Chem Geol 595:120797. https://doi.org/10.1016/j.chemgeo.2022.120797
Lam W-K, Hahn S, Ayanoglu E, Djerassi C (1989) Phospholipid studies of marine organisms. 22. Structure and biosynthesis of a novel brominated fatty acid from a *Hymeniacidonid* sponge. J Org Chem Res 54:3428–3432. https://doi.org/10.1021/jo00275a032
Land LS, Goreau TF (1970) Submarine lithification of Jamaican reefs. J Sediment Petrol 40:457–462
Land LS, Moore CH (1980) Lithification, micritization and syndepositional diagenesis of biolithites on the Jamaican island slope. J Sediment Petrol 50:357–370. https://doi.org/10.1306/212F7A09-2B24-11D7-8648000102C1865D
Lee J-H, Riding R (2018) Marine oxygenation, lithistid sponges, and the early history of Paleozoic skeletal reefs. Earth Sci Rev 181:98–121. https://doi.org/10.1016/j.earscirev.2018.04.003
Litchfield C, Morales RW (1976) Are demospongiae membranes unique among living organisms. In: Harrison FW, Cowden RR (eds) Aspects of sponge biology. Academic Press, New York, pp 183–200
Litchfield C, Greenberg AJ, Noto G, Morales RW (1976) Unusually high levels of C_{24}–C_{30} fatty acids in sponges of the class demospongiae. Lipids 11:567–570. https://doi.org/10.1007/BF02532903
Litchfield C, John T, Virginia D (1980) 5,9,23-triacontatrienoic acid, principal fatty acid of the marine sponge *Chondrilla nucula*. Lipids 15:200–202. https://doi.org/10.1007/BF02540971
Love GD, Grosjean E, Stalvies C, Fike DA, Grotzinger JP, Bradley AS, Kelly AE, Bhatia M, Meredith W, Snape CE, Bowring SA, Condon DJ, Summons RE (2009) Fossil steroids record the appearance of Demospongiae during the Cryogenian period. Nature 457:718–721. https://doi.org/10.1038/nature07673
Lu Y, Sun X, Xu H, Konishi H, Lin Z, Xu L, Chen T, Hao X, Lu H, Peckmann J (2018) Formation of dolomite catalyzed by sulfate-driven anaerobic oxidation of methane: Mineralogical and geochemical evidence from the northern South China Sea. Am Mineral 103:720–734
Luo C, Reitner J (2014) First report of fossil "keratose" demosponges in Phanerozoic carbonates: preservation and 3-D reconstruction. Naturwissenschaften 101:467–477. https://doi.org/10.1007/s00114-014-1176-0
Luo C, Reitner J (2016) 'Stromatolites' built by sponges and microbes—a new type of Phanerozoic bioconstruction. Lethaia 49:555–570. https://doi.org/10.1111/let.12166
Masse JP, Thomassin BA, Acquaviva M (1989) Bioclastic sedimentary environments of coral reefs and lagoon around Mayotte Island (Comoro Archipelago, Mozambique Channel, SW Indian Ocean). J Coast Res 5:419–432
Matthews RK (1966) Genesis of recent lime mud in southern British Honduras. J Sediment Petrol 36:428–454. https://doi.org/10.1306/74D714DD-2B21-11D7-8648000102C1865D
Morales RW, Litchfield C (1976) Unusual C_{24}, C_{25}, C_{26} and C_{27} polyunsaturated fatty acids of the marine sponge *Microciona prolifera*. Biochim Biophys Acta Bioenerg 431:206–216. https://doi.org/10.1016/0005-2760(76)90140-5
Nougier J, Cantagrel JM, Karche JP (1986) The Comores archipelago in the western Indian Ocean: volcanology, geochronology and geodynamic setting. J Afr Earth Sci 5:135–145. https://doi.org/10.1016/0899-5362(86)90003-5
Peckmann J, Thiel V (2004) Carbon cycling at ancient methane–seeps. Chem Geol 205:443–467. https://doi.org/10.1016/j.chemgeo.2003.12.025
Reitner J (1993) Modern cryptic microbialite/metazoan facies from Lizard Island (Great Barrier Reef, Australia) formation and concepts. Facies 29:3–39. https://doi.org/10.1007/BF02536915
Reitner J, Schumann-Kindel G (1997) Pyrite in mineralized sponge tissue—product of sulfate reducing sponge related bacteria? Facies 36:272–284
Reitner J, Gautret P, Marin F, Neuweiler F (1995) Automicrites in a modern marine microbialite—formation model via organic matrices (Lizard Island, Great Barrier Reef, Australia). Bull Inst Océanogr 13:237–263
Reitner J, Thiel V, Zankl H, Michaelis W, Wörheide G, Gautret P (2000) Organic and biogeochemical patterns in cryptic microbialites. In: Riding RE, Awramik SM (eds) Microbial sediments. Springer Berlin Heidelberg, Berlin, pp 149–160
Riding R (1991) Classification of microbial carbonates. Springer, Berlin
Riding R, Tomás S (2005) Stromatolite reef crusts, Early Cretaceous, Spain: Bacterial origin of in situ-precipitated peloid microspar? Sedimentology 53:23–34. https://doi.org/10.1111/j.1365-3091.2005.00751.x
Rubin-Blum M, Antony CP, Sayavedra L, Martínez-Pérez C, Birgel D, Peckmann J, Wu Y-C, Cardenas P, MacDonald I, Marcon Y, Sahling H, Hentschel U, Dubilier N (2019) Fueled by methane: deep-sea sponges from asphalt seeps gain their nutrition from methane-oxidizing symbionts. ISME J 13:1209–1225. https://doi.org/10.1038/s41396-019-0346-7
Rütters H, Sass H, Cypionka H, Rullkötter J (2001) Monoalkylether phospholipids in the sulfate-reducing bacteria *Desulfosarcina variabilis* and *Desulforhabdus amnigenus*. Arch Microbiol 176:435–442. https://doi.org/10.1007/s002030100343
Schlichter D, Fricke HW (1991) Mechanisms of amplification of photosynthetically active radiation in the symbiotic deep-water coral *Leptoseris fragilis*. Hydrobiologia 216:389–394. https://doi.org/10.1007/BF00026491
Seard C, Camoin G, Yokoyama Y, Matsuzaki H, Durand N, Bard E, Sepulcre S, Deschamps P (2011) Microbialite development patterns in the last deglacial reefs from Tahiti (French Polynesia; IODP Expedition #310): Implications on reef framework architecture. Mar Geol 279:63–86. https://doi.org/10.1016/j.margeo.2010.10.013
Taylor J, Parkes RJ (1983) The cellular fatty acids of the sulphate-reducing bacteria, *Desulfobacter* sp. *Desulfobulbus* Sp. and

Desulfovibrio desulfuricans. Microbiology 129:3303–3309. https://doi.org/10.1099/00221287-129-11-3303

Taylor MW, Radax R, Steger D, Wagner M (2007) Sponge-associated microorganisms: Evolution, ecology, and biotechnological potential. Microbiol Mol Biol 71:295–347. https://doi.org/10.1128/MMBR.00040-06

Thiel V, Jenisch A, Wörheide G, Löwenberg A, Reitner J, Michaelis W (1999) Mid-chain branched alkanoic acids from "living fossil" demosponges: a link to ancient sedimentary lipids? Org Geochem 30:1–14. https://doi.org/10.1016/S0146-6380(98)00200-9

Turner EC (2021) Possible poriferan body fossils in early Neoproterozoic microbial reefs. Nature 596:87–91. https://doi.org/10.1038/s41586-021-03773-z

Tzevahirtzian A, Zaragosi S, Bachèlery P, Biscara L, Marchès E (2021) Submarine morphology of the Comoros volcanic Archipelago. Mar Geol 432:106383. https://doi.org/10.1016/j.margeo.2020.106383

UNEP-WCMC, WorldFish Centre, WRI, TNC (2021) Global distribution of warm-water coral reefs, compiled from multiple sources including the Millennium Coral Reef Mapping Project. Version 4.1. Includes contributions from IMaRS-USF and IRD (2005), IMaRS-USF (2005) and Spalding et al. (2001). Cambridge (UK): UN Environment World Conservation Monitoring Centre

Vasconcelos C, McKenzie JA, Bernasconi S, Grujic D, Tiens AJ (1995) Microbial mediation as a possible mechanism for natural dolomite formation at low temperatures. Nature 377:220–222. https://doi.org/10.1038/377220a0

Vinçon-Laugier A, Grossi V, Pacton M, Escarguel G, Cravo-Laureau C (2016) The alkyl glycerol ether lipid composition of heterotrophic sulfate reducing bacteria strongly depends on growth substrate. Org Geochem 98:141–154. https://doi.org/10.1016/j.orggeochem.2016.05.015

Vinçon-Laugier A, Cravo-Laureau C, Mitteau I, Grossi V (2017) Temperature-dependent alkyl glycerol ether lipid composition of mesophilic and thermophilic sulfate-reducing bacteria. Front Microbiol. https://doi.org/10.3389/fmicb.2017.01532

Vinçon-Laugier A, Cravo-Laureau C, Grossi V (2018) Selective preservation among bacterial alkyl glycerol ether lipid structures during long term oxic and anoxic incubation. Org Geochem 125:24–28. https://doi.org/10.1016/j.orggeochem.2018.08.009

Volkman JK (1986) A review of sterol markers for marine and terrigenous organic matter. Org Geochem 9:83–99. https://doi.org/10.1016/0146-6380(86)90089-6

Volkman JK, Jeffrey SW, Nichols PD, Rogers GI, Garland CD (1989) Fatty acid and lipid composition of 10 species of microalgae used in mariculture. J Exp Mar Biol Ecol 128:219–240. https://doi.org/10.1016/0022-0981(89)90029-4

Warthmann R, van Lith Y, Vasconcelos C, McKenzie JA, Karpoff AM (2000) Bacterially induced dolomite precipitation in anoxic culture experiments. Geology 28:1091–1094. https://doi.org/10.1130/0091-7613(2000)28%3c1091:BIDPIA%3e2.0.CO;2

Webster JM, Braga JC, Clague DA, Gallup C, Hein JR, Potts DC, Renema W, Riding R, Riker-Coleman K, Silver E, Wallace LM (2009) Coral reef evolution on rapidly subsiding margins. Glob Planet Change 66:129–148. https://doi.org/10.1016/j.gloplacha.2008.07.010

Wefer G, Berger WH (1991) Isotope paleontology: growth and composition of extant calcareous species. Mar Geol 100:207–248. https://doi.org/10.1016/0025-3227(91)90234-U

Wells JW (1954) Bikini and nearby atolls, Marshall Islands; recent corals of the Marshall Islands. US Geol Surv Prof Pap 260:385–486. https://doi.org/10.3133/pp260I

Wieland A, Pape T, Möbius J, Klock J-H, Michaelis W (2008) Carbon pools and isotopic trends in a hypersaline cyanobacterial mat. Geobiology 6:171–186. https://doi.org/10.1111/j.1472-4669.2007.00138.x

Wijekoon WMD, Ayanoglu E, Djerassi C (1984) Phospholipid studies of marine organisms 9. New brominated demospongic acids from the phospholipids of two *Petrosia* species. Tetrahedron Lett 25:3285–3288. https://doi.org/10.1016/S0040-4039(01)81365-4

Zhang S (2020) The relationship between organoclastic sulfate reduction and carbonate precipitation/dissolution in marine sediments. Mar Geol 428:106284. https://doi.org/10.1016/j.margeo.2020.106284

Zhang F, Xu H, Konishi H, Kemp JM, Roden EE, Shen Z (2012) Dissolved sulfide-catalyzed precipitation of disordered dolomite: Implications for the formation mechanism of sedimentary dolomite. Geochim Cosmochim Acta 97:148–165. https://doi.org/10.1016/j.gca.2012.09.008

Zhang F, Yan C, Teng HH, Roden EE, Xu H (2013) In situ AFM observations of Ca–Mg carbonate crystallization catalyzed by dissolved sulfide: Implications for sedimentary dolomite formation. Geochim Cosmochim Acta 105:44–55. https://doi.org/10.1016/j.gca.2012.11.010

Zhang D, Sun W, Feng G, Zhang F, Anbuchezhian R, Li Z, Jiang Q (2015) Phylogenetic diversity of sulphate-reducing *Desulfovibrio* associated with three South China Sea sponges. Lett Appl Microbiol 60:504–512. https://doi.org/10.1111/lam.12400

Zumberge JA, Love GD, Cárdenas P, Sperling EA, Gunasekera S, Rohrssen M, Grosjean E, Grotzinger JP, Summons RE (2018) Demosponge steroid biomarker 26-methylstigmastane provides evidence for Neoproterozoic animals. Nat Ecol Evol 2:1709–1714. https://doi.org/10.1038/s41559-018-0676-2